Eur. J. Mineral.
2012, **24**, 695–715
Published online March 2012

Li-bearing tourmalines in Variscan granitic pegmatites from the Moldanubian nappes, Lower Austria

ANDREAS ERTL[1,*], RALF SCHUSTER[2], JOHN M. HUGHES[3], THOMAS LUDWIG[4], HANS-PETER MEYER[4], FRIEDRICH FINGER[5], M. DARBY DYAR[6], KATJA RUSCHEL[1], GEORGE R. ROSSMAN[7], URS KLÖTZLI[8], FRANZ BRANDSTÄTTER[9], CHRISTIAN L. LENGAUER[1] and EKKEHART TILLMANNS[1]

[1] Institut für Mineralogie und Kristallographie, Geozentrum, Universität Wien, Althanstrasse 14, 1090 Wien, Austria
*Corresponding author, e-mail: andreas.ertl@a1.net
[2] Geologische Bundesanstalt (Geological Survey), Neulinggasse 38, 1030 Wien, Austria
[3] Department of Geology, University of Vermont, Burlington, VT 05405, USA
[4] Institut für Geowissenschaften, Im Neuenheimer Feld 236, 69120 Heidelberg, Germany
[5] Fachbereich Materialforschung & Physik, Universität Salzburg, Hellbrunnerstrasse 34, 5020 Salzburg, Austria
[6] Department of Astronomy, Mount Holyoke College, South Hadley, MA 01075, USA
[7] Division of Geological and Planetary Sciences, California Institute of Technology, Pasadena, CA 91125-2500, USA
[8] Department of Lithospheric Research, Geozentrum, Universität Wien, Althanstrasse 14, 1090 Wien, Austria
[9] Mineralogisch-Petrographische Abteilung, Naturhistorisches Museum, 1010 Wien, Austria

Abstract: Crystal structures, chemical (including light elements) and spectral data (optical and Mössbauer spectroscopies) were used to characterize coloured (brown, pink, green) tourmalines from three granitic pegmatites from the Moldanubian nappes (Königsalm, Maigen and Blocherleitengraben; Lower Austria). The tourmalines can be classified as fluor-schorl, schorl, foitite, magnesiofoitite, olenite and ''fluor-elbaite'' with varying Li contents, up to ~1.2 wt% Li_2O. Coexisting minerals are quartz, plagioclase (up to An_7), microcline, garnet (spessartine-almandine), muscovite, biotite (annite), very rare lepidolite, apatite, monazite-(Ce), xenotime-(Y), allanite-(Ce) and zircon. The chemical composition of the Fe^{2+}-rich tourmaline samples (up to ~1.0 wt% TiO_2) varies from fluor-schorl, with $a = 15.987(2)$, $c = 7.163(2)$ Å to $^{X}(\square_{0.63}Na_{0.37})$ $^{Y}(Fe^{2+}{}_{1.12}Al_{1.09}Mg_{0.56}Mn^{2+}{}_{0.08}Fe^{3+}{}_{0.07}Li_{0.02}Ti^{4+}{}_{0.01}Zn_{0.01}\square_{0.04})$ $^{Z}(Al_{5.74}Mg_{0.26})$ $(BO_3)_3$ $[Si_{5.96}Al_{0.04}O_{18}]$ $^{V}(OH)_3$ $^{W}[(OH)_{0.95}F_{0.05}]$, strongly dichroic (pink and blue) foitite, with $a = 15.9537(2)$, $c = 7.1448(4)$ Å, to $^{X}(\square_{0.51}Na_{0.49})$ $^{Y}(Fe^{2+}{}_{0.97}Al_{0.93}Mg_{0.75}Fe^{3+}{}_{0.23}Mn^{2+}{}_{0.04}Li_{0.01}Ti^{4+}{}_{0.01}\square_{0.06})$ $^{Z}(Al_{5.72}Mg_{0.28})$ $(BO_3)_3$ $[Si_{5.95}Al_{0.05}O_{18}]$ $^{V}(OH)_3$ $^{W}[(OH)_{0.91}O_{0.06}F_{0.03}]$, magnesiofoitite, with $a = 15.9476(4)$, $c = 7.1578(4)$ Å. The chemical composition of the Al- and Li-rich and Mn^{2+}-bearing (up to ~5.7 wt% MnO) samples varies from $^{X}(Na_{0.84}Ca_{0.02}\square_{0.14})$ $^{Y}(Al_{1.35}Li_{0.78}Mn^{2+}{}_{0.65}Ti^{4+}{}_{0.01}\square_{0.21})$ $^{Z}Al_6$ $(BO_3)_3$ $[Si_{5.92}Al_{0.04}B_{0.04}O_{18}]$ $^{V}(OH)_3$ $^{W}[F_{0.81}(OH)_{0.19}]$, ''fluor-elbaite'' with $a = 15.8887(3)$, $c = 7.1202(3)$ Å, to $^{X}(Na_{0.76}Ca_{0.12}\square_{0.12})$ $^{Y}(Al_{1.52}Li_{0.69}Mn^{2+}{}_{0.43}Fe^{2+}{}_{0.09}\square_{0.27})$ $^{Z}Al_6$ $(BO_3)_3$ $[Si_{5.71}B_{0.29}O_{18}]$ $^{V}(OH)_3$ $^{W}[F_{0.69}(OH)_{0.31}]$, B-rich ''fluor-elbaite'', with $a = 15.8430(3)$, $c = 7.1051(3)$ Å. A positive correlation between the <*T*-O> and <*Z*-O> bond lengths in tourmalines where the *Z* site is only occupied by Al ($R^2 = 0.617$) is useful to correct the <*Z*-O> bond length for the inductive effect of the varying <*T*-O> bond length. This is important for producing accurate assignments for the different 6-coordinated sites in tourmaline.

On the basis of Sm-Nd (garnet, monazite), U-Th-Pb, and U-Pb ages (monazite), the pegmatites crystallised during the Variscan tectonometamorphic event in the Visean (339 ± 4 Ma Maigen, 332 ± 3 Ma Königsalm). These ages are in the range of the earliest intrusions of the South Bohemian pluton (Rastenberg type durbachites). However, on the basis of the spatial relationship of the pegmatites and the Rastenberg type intrusions, a linkage of the intrusive body and the pegmatites is unlikely. Alternatively, the pegmatites may have evolved as granitic pegmatitic melts during decompression from the surrounding country rocks in the frame of exhumation of the Moldanubian nappes after the peak of the Variscan metamorphism.

Key-words: Li-bearing tourmaline, granitic pegmatite, Moldanubian nappes, chemical analyses, crystal structure, geochronology.

1. Introduction

Tourmaline is a silicate mineral group with a highly complex crystal structure and a large variety of chemical compositions. The general chemical formula of the tourmaline-group minerals is $X\ Y_3\ Z_6\ [T_6O_{18}]\ (BO_3)_3\ V_3\ W$ (Henry *et al*., 2011). Because of the potential of tourmaline to incorporate numerous elements, detailed characterisation requires several different investigations (electron microprobe, optical, crystal structure refinement, and Mössbauer spectroscopic measurements) that sometimes yield surprising results.

0935-1221/12/0024-2203 $ 9.45
DOI: 10.1127/0935-1221/2012/0024-2203

The composition of tourmaline is dependent on the temperature and pressure as well as the chemical composition of the magmatic or metamorphic environment where the tourmaline formed (*e.g.*, Henry & Dutrow, 1996; Ertl *et al.*, 2010a and b). Therefore the composition bears information that is essential to resolve many petrological questions. When tourmaline crystallises from pegmatitic melts, the relation of the tourmaline crystal chemistry to the composition of the parent melt is not well understood. However, the complex zoning of tourmalines reflects the evolution of the pegmatitic melt which may change rapidly by processes such as fractional crystallisation, mixing of melt fractions, or interaction with the wall rock (*e.g.*, Ertl *et al.*, 2010c).

In the last decades, pink-to-green coloured tourmalines were found in several pegmatites of granitic composition occurring in the southern part of the Bohemian massif in Lower Austria. The pegmatits are situated in the Moldanubian nappes, which formed during the Variscan tectonometamorphic event in Carboniverous times. From the Moldanubian nappes only Mn-rich and Li-bearing, pink-brown to yellow-brown tourmaline from a pegmatite of the Drosendorf unit, near the village Eibenstein an der Thaya (Ertl *et al.*, 2003a, 2004b) has been described in detail until now. The host pegmatite crystallised at 337 ± 4 Ma and is characterised by initial Sr and Nd isotopic ratios that do not fit the contemporaneous granitic intrusions of the Bohemian massif.

In this paper, we examine the crystal structure, chemistry, and spectroscopy of coloured tourmaline and chemical data of coexisting minerals from three additional granitic pegmatites from the Moldanubian nappes. They are located at Königsalm, Maigen and Blocherleitengraben, in the area northwest of Krems an der Donau (Lower Austria). Additionally, we determined the time of crystallisation of two of the investigated pegmatites by Sm-Nd analyses on garnet, feldspar, monazite and xenotime and by a chemical U-Th-Pb monazite age. On the basis of mineralogy, chemistry, and the crystallisation ages, the evolution of the pegmatites is discussed in the framework of the geodynamic history of the Bohemian massif.

2. Regional geology

The southern part of the Bohemian massif was consolidated during the Variscan tectonometamorphic event (380–300 Ma) and comprises the Moravo-Silesicum and the Moldanubicum (Fig. 1; *e.g.*, Fuchs & Matura, 1976; Klötzli *et al.*, 1999; Neubauer & Handler, 2000; Finger *et al.*, 2007). The nappes of the Moravo-Silesicum (Moravian nappes) are composed of crustal material with a Cadomian imprint (at *ca.* 600 Ma), and show a greenschist to amphibolite facies Variscan metamorphic overprint. The Moldanubicum is overlying with a west-dipping thrust plane. It can be subdivided into the Moldanubian nappes, the Bavarian massif and the South Bohemian Batholith (Fuchs & Matura, 1976; Finger *et al.*, 2007). The Moldanubian nappes show a succession from bottom to top (Fig. 1b): the Ostrong nappe built up mostly by paragneisses (''Monotonous Series''), the Mühldorf nappe composed of the Drosendorf unit (''Varied Series'') and the Dobra orthogneiss, the Gföhl nappe comprising the Gföhl orthogneiss as well as paragneisses and amphibolites (Raabs unit), and the uppermost Granulite nappe built up by granulites with lenses of basic and ultrabasic rocks (Neubauer & Handler, 2000). Variscan metamorphism within the Moldanubian nappes is polyphase and reached amphibolite, granulite and partly eclogite facies conditions (Carswell, 1991; Carswell & O'Brien, 1991, 1993; Petrakakis, 1997). Post nappe stacking, the South Bohemian Batholith intruded the Moldanubian nappes in Late Carboniferous time between 335 and 300 Ma. The latter can be subdivided in a sequence of several intrusive suites, including I-type and S-type granites. Towards the west, the Moldadanubian nappes show an intense, high-temperature (H*T*), low-pressure (L*P*) overprint with migmatisation and the formation of S-type intrusions at 325–320 Ma. The internal structure is obscured in this part, which is referred to the Bavarian massif (Fuchs & Matura, 1976; Finger *et al.*, 2007; Linner, 2007).

The tectonic evolution of the Variscan orogen in central Europe is complex and contains many open questions. A recent summary is given in Kroner *et al.* (2008). An interpretation of the geology in the southern part of the Bohemian massif can be found in Finger *et al.* (2007). The early stages of nappe stacking in the Moldanubicum are documented by relics of a pressure-dominated metamorphism. Prince *et al.* (2000) and Svojtka *et al.* (2002) reported Sm-Nd garnet ages of 354 ± 6 Ma. These garnets are interpreted as high-*P* and high-*T* phases formed during the granulite evolution. Peak metamorphism occurred just before the termination of the Intramoldanubian nappe stacking at about 340 Ma. After that, a strong L*P*–H*T* regional metamorphism at about 340–335 Ma occurred, which may be an expression of increased mantle heat flow after slab break-off (Finger *et al.*, 2007). Medaris *et al.* (1990) summarised the available Sm-Nd ages of peridotites and associated H*P* mafic rocks from the Gföhl nappe. The garnet peridotites constrain ages of 339 ± 10 Ma, and garnet pyroxenite and eclogites yielded similar Sm-Nd ages of 336 ± 7 Ma, interpreted as high temperature cooling ages. Intramoldanubian nappe-stacking is postdated by the intrusion of the South Bohemian Pluton that took place between 335 and 300 Ma (Klötzli *et al.*, 1999), and by the thrusting of the Moldanubian nappes onto the foreland in the east, which caused the formation and incorporation of the Moravian nappes into the Variscan orogen. In the western part of the Bohemian massif, an event of intense migmatisation and anatectic melting affected the Moldanubian nappes at 325–320 Ma (Tropper *et al.*, 2006), causing the formation of the Bavarian massif. On the basis of Ar-Ar and Rb-Sr mica ages, regional cooling of the Moldanubicum is earlier in the east and becomes younger towards the west. At the margin towards the Moravian nappes, Ar-Ar muscovite ages of about 325 Ma have been measured, whereas at the southwestern margin

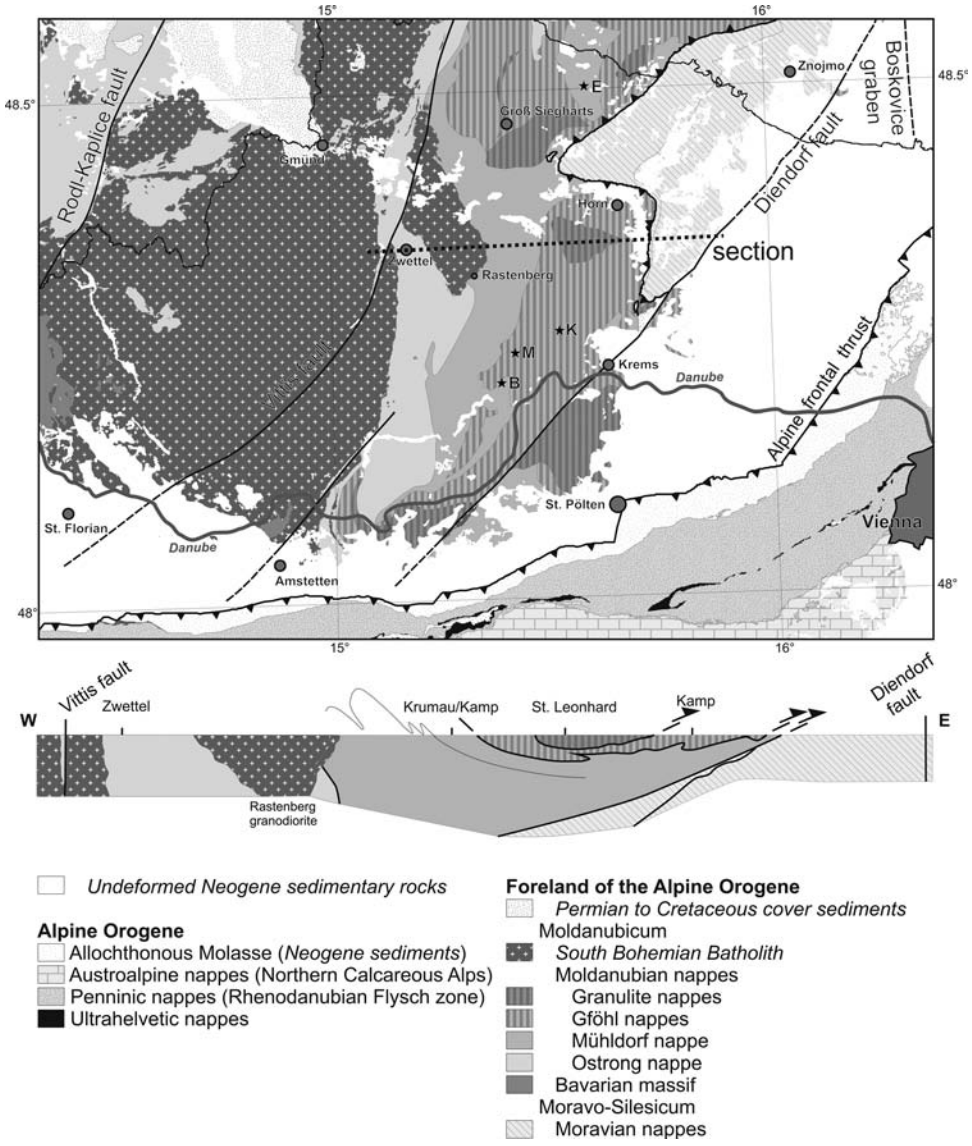

Fig. 1. Simplified geological map showing the southern part of the Bohemian massif with the sample localities (K, Königsalm; M, Maigen; B, Blocherleitengraben; E, Eibenstein). A section according to Matura (2003) is also shown.

of the Bohemian massif ages decrease to less than 300 Ma (Dallmeyer *et al*., 1992; Frank & Scharbert, 1993).

2.1. Description of the investigated pegmatites

The pegmatites investigated during this study are from a relatively small area (7 × 14 km) northwest of Krems an der Donau (Lower Austria). Two of the pegmatites are situated within the Gföhl nappe, which consists of the Gföhl orthogneiss and associated paragneisses, and the amphibolites of the Raabs unit. The orthogneiss developed from Ordovician acidic volcanic rocks (Frank *et al*., 1990; Klötzli *et al*., 1999). The third pegmatite is embedded in paragneisses and calc-silicate rock of the Drosendorf unit (''Varied Series'') that build up the Mühldorf nappe.

2.1.1. Pegmatite Königsalm

The Königsalm pegmatite (WGS84 N 48°28′21″/E 015°31′09″), located ∼3.5 km northwest to the village Senftenberg, is embedded in Gföhl orthogneiss of the Gföhl nappe. A quarry (left open) is situated in the more than 10 m thick pegmatite lens which shows discordant contacts to the country rocks. Tourmaline occurs in black, pale-blue, pale-green, brownish, and pink colours. To date, only the pale-blue to pale-green tourmaline, which occurs as thin fibres (tourmaline-asbestos; Meixner, 1981), has been investigated by Ertl (1995). Based only on the lattice parameters of $a = 15.926(2)$ and $c = 7.198(1)$ Å, this tourmaline was identified as a dravite. With respect to the colour, black tourmaline was identified as schorl by Sigmund (1937). It forms crystals up to ∼17 cm in length and ∼8 cm in diameter that have been found in pockets

(Niedermayr, 1969). Pink coloured, translucent tourmaline that occurs as small columnar crystals was also mentioned by Sigmund (1937). Associated minerals are quartz (also as smoky quartz crystals in pockets, up to ~25 cm in lengths), microcline, albite, muscovite, biotite, pale-green and colourless apatite (Himmelbauer, 1929; Sigmund, 1937), ilmenite, yellowish-brown to greenish-brown xenotime (Meixner, 1965; Niedermayr, 1969), reddish-brown monazite, zircon (Kontrus & Niedermayr, 1969), spessartine-almandine, zoisite (Niedermayr, 1969), pale-pink apatite (found in pockets, crystals up to 4 cm in diameter), ferrocolumbite (Koller, 1974) and rose quartz (Huber & Huber, 1977). In some zones, biotite occurs as 0.2–2 mm thick books up to 10 cm wide, intergrown with feldspar and muscovite flakes up to 5 mm wide. In these zones, millimetre-sized idioblastic monazite and xenotime often occur at the interfaces between biotite and feldspar. Garnet is present as idioblastic crystals within the pockets, but is more frequent within feldspar and quartz-rich domains. Sometimes it occurs in up to 3 cm aggregates composed of garnet and quartz, within a mass of yellowish feldspar.

2.1.2. Pegmatite Maigen

The pegmatite at the small village of Maigen (WGS84 N 48°26′25″/E 015°24′44″), near the village Weinzierl am Walde, is embedded in a biotite-bearing paragneiss of the Gföhl nappe. The pegmatite lens with ~15 × 20 m in size occurs in a cornfield (called ''Tannfeld''). Tourmaline occurs in black, pale-green to dark-green, and rarely pale-pink colours. Black tourmaline was identified as schorl and the coloured tourmaline as Mn-bearing elbaite and olenite (based on lattice parameters and semi-quantitative chemical data, without F, B, Li, or H analyses; Ertl, 1995). Associated minerals in this pegmatite are quartz, albite, apatite (pale-blue, green, colourless), stilbite (Kappelmüller, 1994), K-feldspar, spessartine-almandine, muscovite and lepidolite (associated with pink elbaite), which rarely occurs in crystal aggregates up to ~1 cm in size (Ertl, 1995). Crystals of dark-green tourmaline, intergrown with quartz and feldspar, can reach ~3 cm in length and ~1.5 cm in diameter, whereas pale-pink elbaite reaches up to ~2 cm in length and ~1.5 cm in diameter (Ertl, 1995). The largest elbaite crystals from Austria have been found at this locality. Garnet is present as millimetre-sized crystals intergrown with feldspar and quartz.

2.1.3. Pegmatite Blocherleitengraben

The pegmatite in the upper Blocherleitengraben (WGS84 N 48°23′42″/E 015°24′05″) crops out in the Miesling valley, ~4 km to the north of the village Spitz. This pegmatite is situated in the Mühldorf nappe, embedded in paragneisses and calc-silicate rock of the Drosendorf unit (''Varied Series''). Pegmatite blocks up to 5 m^3 in size occur in the wood in an area of several hundred m^2. Tourmaline occurs in black, red (Knobloch, 1982), greenish-brown, reddish-brown and pink colours (Ertl, 1995). Black tourmaline was identified as schorl and coloured tourmaline (reddish crystals reach up to 3 × 8 mm in size) in small miarolitic cavities was identified as elbaite (based on lattice parameters and semi-quantitative chemical data, without F, B, Li, or H analyses; Ertl, 1995). Associated minerals in this pegmatite are quartz (crystals up to a few cm), albite, biotite, pyrite, magnetite (Kappelmüller, 1994), orange-coloured spessartine (up to ~2 cm in diameter), K-feldspar, montmorillonite and zircon (Ertl, 1995). Pyrophanite exsolution lamellae (up to ~20 μm in length) in magnetite and also pyrophanite (in size of ~60 μm) intimately intergrown with spessartine and magnetite were also described (Hehenberger, 1996).

3. Sample selection and analytical techniques

3.1. Sample selection

Pegmatite samples that were collected in 1980 at Königsalm show miarolitic cavities up to ~1 cm in diameter, which contain, in addition to small albite crystals, black-to-brownish tourmaline crystals up to ~5 mm in length. One brownish tourmaline crystal ~230 × 300 μm in size (TK12) was separated and used for structure characterisation and subsequent chemical analyses. In similar pockets, tourmaline crystals up to ~1 cm in length and up to ~1 mm in diameter were found in 2000. These crystals show pink zones and split in several parallel brownish-green needles with a diameter of ~50 μm. Crystal fragments of the pink (TK3; 200 × 250 μm) and the brownish-green zone (TK42; 50 × 130 μm) were separated for further investigations. For Sm-Nd age determinations, garnet and feldspar were separated from a sample (EK1) consisting of *ca.* 2 cm aggregates of garnet and quartz within a matrix of massive, slightly yellowish feldspar. Idioblastic monazite and xenotime crystals, each about 1.5 mm in size, were taken from sample EK2 composed of centimetre sized biotite books intergrown with feldspar and muscovite. Some of these crystals were used for U-Th-Pb and U-Pb age dating.

Samples from the pegmatite collected in 1988 at Maigen contain coloured tourmaline crystals intergrown with feldspar and quartz. Crystal fragments were separated from a dark green tourmaline crystal ~1.5 × 4 mm in size (MAG; 200 × 200 μm), and from the rim of a pale-pink tourmaline crystal ~5 × 8 mm in size (MAP12; 180 × 180 μm). In 1994, small miarolitic cavities (a few cm in diameter) with black tourmalines and smoky quartz crystals were found in this pegmatite. The rim of a black tourmaline, 9 × 13 mm in width and 8 mm in length, well crystallised, with the prismatic forms {10-10}, {11-20}, pyramidal forms {01-12}, {10-11}, and {0001} (pedion), was separated for investigations (MASR; 250 × 500 μm). Garnet and feldspar for Sm-Nd analyses were separated from sample EM1, which consists of xenoblastic garnet up to 1 mm in diameter, plagioclase and quartz.

In the pegmatite at Blocherleitengraben, tiny miarolitic cavities with tourmaline crystals were found in 1982. Here

we investigate a ∼1 mm rim, consisting of a pink (outside rim; BLP1; 200 × 250 μm) and a greenish-brown zone (BLG1; 200 × 500 μm), grown over a schorl crystal (∼2 cm in diameter). Most of the schorl crystal is embedded in quartz; only a small part (∼5 × 5 mm) was growing inside the cavity and overgrown by the described coloured tourmaline. Nd isotopic data were measured on a single feldspar crystal (sample EB1).

3.2. Crystal structure

Tourmaline crystals were mounted on a Bruker Apex CCD diffractometer equipped with graphite-monochromatic Mo$K\alpha$ radiation. Refined cell-parameters and other crystal data are listed in Table 1. Redundant data were collected for an approximate sphere of reciprocal space, and were integrated and corrected for Lorentz and polarisation factors using the Bruker program SAINTPLUS (Bruker AXS Inc. 2001). The structure was refined using the tourmaline starting model and the Bruker SHELXTL V. 6.10 package of programs, with neutral-atom scattering factors and terms for anomalous dispersion. Refinement was performed with anisotropic displacement parameters for all non-hydrogen atoms. Atomic parameters are listed in Table 2, anisotropic displacement parameters in Table S1, freely available online as Supplementary Material linked to this article on the GSW website of the journal, http://eurjmin.geoscience world.org/. and selected interatomic distances in Table 3.

3.3. Chemical analyses

The tourmaline single crystals and crystal fragments used for the structure refinement were prepared as a section (polished on one side of the samples) for chemical analysis. Concentrations of all elements except B, Li, Be, and H were determined with a Cameca SX51 electron microprobe (EPMA) equipped with five wavelength-dispersive spectrometers (Universität Heidelberg). Concentrations of H, Li, Be and B were determined by secondary ion mass spectrometry (SIMS) with a CAMECA IMS 3f ion microprobe (Universität Heidelberg). All analytical details are given in Ertl *et al.* (2009). Table 4 contains complete chemical-analytical data for the tourmalines.

For an independent determination of the OH content of the tourmaline samples TK3 and TK42, ∼14 mg of these samples were used for thermogravimetric analysis (TGA), which was performed on a Mettler-Toledo TGA/SDTA 851 instrument (Universität Wien). The powder was heated from 25°C to 1100°C (5°C/min) under a stream of N_2 gas (gas flow: 25 ml/min).

X-ray energy dispersive (EDS) analyses of feldspar, garnet and mica were obtained with an analytical SEM (JEOL-JSM 6400 equipped with a KEVEX detector) at the Mineralogisch-Petrographische Abteilung, Naturhistorisches Museum, Wien, Austria. Representative EDS analyses of these minerals are given in Tables S2 and S3.

Table 1. Sample parameters and refinement results for tourmalines from the Moldanubicum, Lower Austria.

	TK12	TK3	TK42	MASR	MAG	MAP12	BLG1	BLP1
a, c (Å)	15.987(2), 7.163(2)	15.9537(4), 7.1448(4)	15.9476(4), 7.1578(4)	15.9783(3), 7.1507(2)	15.8830(3), 7.1093(2)	15.8887(3), 7.1202(3)	15.9107(3), 7.1267(3)	15.8430(3), 7.1051(3)
h, k, l ranges	−22/22, −22/22, −10/10	−22/22, −22/22, −10/10	−22/22, −22/22, −10/10	−22/22, −22/22, −10/10	−22/22, −22/22, −9/9	−22/22, −22/22, −10/9	−22/22, −22/22, −10/10	−22/22, −22/22, −9/9
Total reflections measured	10,060	9,862	10,143	11,677	9,958	9,938	10,026	9,818
Unique reflections	1134	1123	1122	1131	1107	1108	1111	1109
$R1(F)$, $wR2_{all}(F^2)$	1.53%, 4.10%	1.62%, 4.46%	2.18%, 5.46%	1.30%, 3.58%	1.43%, 3.98%	1.69%, 4.52%	1.80%, 4.87%	1.84%, 4.83%
R_{int}	1.16%	3.12%	2.77%	1.60%	1.69%	1.68%	2.45%	2.20%
Flack x parameter	−0.003(14)	−0.00(2)	0.04(3)	−0.01(1)	−0.33(6)	−0.08(11)	−0.38(6)	−0.04(13)
'Observed' refls.	1134	1123	1120	1131	1107	1108	1111	1109
Extinct. coefficient	0.0015(3)	0.0010(3)	0.00000(19)	0.0027(2)	0.0006(3)	0.0000(3)	0.0000(3)	0.0000(2)
No. of refined parameters	96	98	95	95	98	94	94	96
GooF	1.134	1.128	1.146	1.123	1.162	1.107	1.098	1.096
$\Delta\sigma_{min}$, $\Delta\sigma_{max}$ (e/Å^3)	−0.38, 0.37	−0.32, 0.27	−0.38, 0.46	−0.21, 0.44	−0.21, 0.45	−0.48, 0.71	−0.48, 0.74	−0.36, 0.55

Table 2. Positional parameters and $U_{equivalent}$ for atoms of tourmalines from the Moldanubicum, Lower Austria.

Site	TK12	TK3	TK42	MASR	MAG	MAP12	BLG1	BLP1
X								
x	0	0	0	0	0	0	0	0
y	0	0	0	0	0	0	0	0
z	0.2498(3)	0.2498(8)	0.2494(9)	0.7500(4)	−0.2500(4)	0.2495(3)	0.7501(3)	0.7501(3)
occ.	$Na_{0.81(1)}$	$Na_{0.40(1)}$	$Na_{0.53(1)}$	$Na_{0.62(1)}$	$Na_{0.65(1)}$	$Na_{0.90(1)}$	$Na_{0.99(1)}$	$Na_{0.96(1)}$
U_{eq}	0.0249(8)	0.0297(18)	0.0308(18)	0.0277(10)	0.0269(8)	0.0268(7)	0.0255(7)	0.0244(6)
Y								
x	0.12555(3)	0.12457(3)	0.12456(5)	−0.12436(2)	−0.12248(4)	0.12373(6)	−0.12380(5)	−0.12331(6)
y	½ *x*	½ *x*	½ *x*	½ *x*	½ *x*	½ *x*	½ *x*	½ *x*
z	−0.35054(4)	−0.35730(6)	−0.35953(9)	0.34676(4)	0.34775(7)	−0.3567(1)	0.35847(9)	0.3502(1)
occ.	$Al_{0.411(4)}Fe_{0.589}$	$Al_{0.631(4)}Fe_{0.369}$	$Al_{0.628(5)}Fe_{0.372}$	$Al_{0.410(4)}Fe_{0.590}$	$Al_{0.896(3)}Fe_{0.104}$	$Al_{0.913(5)}Li_{0.087}$	$Al_{0.854(4)}Fe_{0.146}$	$Al_{0.857(6)}Li_{0.143}$
U_{eq}	0.01047(12)	0.01059(15)	0.0102(2)	0.0105(1)	0.0112(7)	0.0111(2)	0.112(2)	0.0120(3)
Z								
x	0.29863(3)	0.29815(3)	0.29816(4)	−0.29837(3)	−0.29724(3)	0.29754(3)	−0.29702(4)	−0.29737(3)
y	0.26179(3)	0.26147(3)	0.26145(4)	−0.26159(3)	−0.26071(3)	0.26074(3)	−0.26092(4)	−0.26055(4)
z	−0.36581(5)	−0.37335(6)	−0.37657(8)	0.36438(5)	0.36897(5)	−0.37275(6)	0.37126(7)	0.37027(7)
occ.	$Al_{1.00}$	$Al_{1.00}$	$Al_{1.00}$	$Al_{0.966(3)}Fe_{0.034}$	$Al_{1.00}$	$Al_{1.00}$	$Al_{1.00}$	$Al_{1.00}$
U_{eq}	0.0070(1)	0.0078(1)	0.0065(1)	0.0076(1)	0.00770(9)	0.0079(1)	0.0077(1)	0.0091(1)
T								
x	0.01919(2)	0.19187(3)	0.19193(4)	−0.19190(2)	−0.19185(2)	0.19192(3)	−0.19192(3)	−0.19175(3)
y	0.18998(3)	0.18986(3)	0.18994(4)	−0.18991(2)	−0.18983(2)	0.18998(3)	−0.19002(3)	−0.18986(3)
z	0.02289(5)	0.01622(6)	0.01238(8)	−0.02552(5)	−0.02240(5)	0.01580(6)	−0.01710(6)	−0.01896(6)
occ.	$Si_{1.00}$	$Si_{1.00}$	$Si_{1.00}$	$Si_{1.00}$	$Si_{1.00}$	$Si_{1.00}$	$Si_{1.00}$	$Si_{0.933(5)}B_{0.067}$
U_{eq}	0.0078(1)	0.0070(1)	0.0060(1)	0.00700(9)	0.00710(8)	0.0067(1)	0.0067(3)	0.0067(2)
B								
x	0.11023(8)	0.11010(9)	0.1102(1)	0.11018(7)	−0.10962(7)	0.10962(9)	−0.10992(9)	−0.10955(9)
y	2*x*	2*x*	2*x*	2*x*	2*x*	2*x*	2*x*	2*x*
z	0.4774(3)	0.4713(3)	0.4669(5)	0.4798(3)	−0.4750(3)	0.4707(3)	−0.4721(3)	−0.4732(3)
occ.	$B_{1.00}$	$B_{1.00}$	$B_{1.00}$	$B_{1.00}$	$B_{1.00}$	$B_{1.00}$	$B_{1.00}$	$B_{1.00}$
U_{eq}	0.0100(3)	0.0094(4)	0.0098(5)	0.0091(3)	0.0087(3)	0.0083(4)	0.0084(4)	0.0098(4)
O1								
x	0	0	0	0	0	0	0	0
y	0	0	0	0	0	0	0	0
z	−0.1934(4)	−0.2093(7)	−0.2110(6)	0.1948(4)	0.2050(5)	−0.2010(5)	0.1984(5)	0.1990(5)
occ.	$F_{0.86(8)}O_{0.14}$	$O_{1.00}$	$O_{1.00}$	$O_{1.00}$	$O_{1.00}$	$F_{1.00}$	$F_{1.00}$	$F_{0.83(9)}O_{0.17}$
U_{eq}	0.041(1)	0.028(1)	0.0256(9)	0.0332(7)	0.0288(8)	0.058(1)	0.061(1)	0.050(2)
H1								
x	–	0.0298(89)	–	–	0.0186(34)	–	–	–
y	–	0.0149(44)	–	–	0.0373(70)	–	–	–
z	–	−0.169(15)	–	–	0.182(14)	–	–	–
occ.	–	0.134(30)	–	–	0.129(27)	–	–	–
U_{eq}	–	0.000(34)	–	–	0.000(25)	–	–	–
O2								
x	0.06176(5)	0.06188(6)	0.06173(8)	−0.06174(5)	−0.06098(5)	0.06081(6)	−0.06107(7)	−0.06057(7)
y	2*x*	2*x*	2*x*	2*x*	2*x*	2*x*	2*x*	2*x*
z	0.5069(2)	0.5054(2)	0.5011(3)	−0.5119(2)	0.5092(2)	0.4997(3)	0.5000(3)	0.4959(3)
occ.	$O_{1.00}$	$O_{1.00}$	$O_{1.00}$	$O_{1.00}$	$O_{1.00}$	$O_{1.00}$	$O_{1.00}$	$O_{1.00}$
U_{eq}	0.0172(3)	0.0172(4)	0.0165(5)	0.0174(3)	0.0178(3)	0.0203(4)	0.0198(4)	0.0205(4)
O3								
x	0.2695(1)	0.2661(1)	0.2660(2)	−0.2675(1)	−0.2639(1)	0.2681(1)	−0.2688(1)	−0.2668(1)
y	1/2*x*	1/2*x*	1/2*x*	1/2*x*	1/2*x*	1/2*x*	1/2*x*	1/2*x*
z	−0.4669(2)	−0.4746(2)	−0.4770(3)	0.4656(2)	0.4703(2)	−0.4746(2)	0.4728(2)	0.4716(2)
occ.	$O_{1.00}$	$O_{1.00}$	$O_{1.00}$	$O_{1.00}$	$O_{1.00}$	$O_{1.00}$	$O_{1.00}$	$O_{1.00}$
U_{eq}	0.0144(3)	0.0138(2)	0.0131(4)	0.0142(3)	0.0145(3)	0.0132(3)	0.0118(3)	0.0147(3)
H3								
x	0.270(3)	0.257(3)	0.263(4)	0.268(3)	−0.258(3)	0.266(3)	−0.268(3)	−0.266(3)
y	1/2*x*	1/2*x*	1/2*x*	1/2*x*	1/2*x*	1/2*x*	1/2*x*	1/2*x*
z	−0.585(6)	−0.605(6)	−0.577(7)	0.584(6)	0.591(5)	−0.588(5)	0.590(6)	0.585(6)
U_{iso}	0.19(4)	0.038(11)	0.04(2)	0.06(1)	0.046(1)	0.019(8)	0.027(10)	0.041(12)
O4								
x	0.09310(5)	0.09376(6)	0.09352(8)	−0.09342(5)	−0.09416(5)	0.09330(6)	−0.09313(6)	−0.09332(6)
y	2*x*	2*x*	2*x*	2*x*	2*x*	2*x*	2*x*	2*x*

Table 2. Continued.

Site	TK12	TK3	TK42	MASR	MAG	MAP12	BLG1	BLP1
z	0.0914(2)	0.0841(2)	0.0807(3)	0.0939(2)	−0.0941(2)	0.0874(2)	−0.0883(2)	−0.0911(2)
occ.	$O_{1.00}$	$O_{1.00}$	$O_{1.00}$	$O_{1.00}$	$O_{1.00}$	$O_{1.00}$	$O_{1.00}$	$O_{1.00}$
U_{eq}	0.0125(3)	0.0118(3)	0.0110(4)	0.0120(3)	0.0118(2)	0.0103(3)	0.0102(3)	0.0121(3)
O5								
x	0.1868(1)	0.1878(1)	0.1872(2)	0.1875(1)	−0.1879(1)	0.18669(1)	−0.1864(1)	−0.1864(1)
y	1/2*x*	1/2*x*	1/2*x*	1/2*x*	1/2*x*	1/2*x*	1/2*x*	1/2*x*
z	0.1142(2)	0.1071(2)	0.1040(3)	0.1170(2)	−0.1166(2)	0.1095(2)	−0.1100(2)	−0.1129(2)
occ.	$O_{1.00}$	$O_{1.00}$	$O_{1.00}$	$O_{1.00}$	$O_{1.00}$	$O_{1.00}$	$O_{1.00}$	$O_{1.00}$
U_{eq}	0.0127(3)	0.0117(3)	0.0105(4)	0.0121(2)	0.0125(2)	0.0107(3)	0.0107(3)	0.0125(3)
O6								
x	0.19796(7)	0.19738(8)	0.1974(1)	−0.19775(7)	−0.19581(6)	0.19673(8)	−0.19727(8)	−0.19609(8)
y	0.18793(7)	0.18678(8)	0.1867(1)	−0.1873(7)	−0.18530(7)	0.18670(8)	−0.18731(8)	−0.18609(8)
z	−0.2011(1)	−0.2082(2)	−0.2119(2)	0.1995(1)	0.2039(1)	−0.2086(2)	0.2073(2)	0.2057(2)
occ.	$O_{1.00}$	$O_{1.00}$	$O_{1.00}$	$O_{1.00}$	$O_{1.00}$	$O_{1.00}$	$O_{1.00}$	$O_{1.00}$
U_{eq}	0.0110(2)	0.0103(2)	0.0098(3)	0.0105(2)	0.0104(2)	0.0099(2)	0.0098(2)	0.0110(2)
O7								
x	0.28509(7)	0.28534(8)	0.2851(1)	−0.28539(6)	−0.28642(6)	0.28577(7)	−0.28555(8)	−0.28568(8)
y	0.28556(7)	0.28581(7)	0.2856(1)	−0.28590(6)	−0.28647(6)	0.28582(7)	−0.28580(8)	−0.28563(7)
z	0.1028(1)	0.0950(2)	0.0914(2)	−0.1043(1)	−0.0997(1)	0.0959(1)	−0.0974(2)	−0.0981(1)
occ.	$O_{1.00}$	$O_{1.00}$	$O_{1.00}$	$O_{1.00}$	$O_{1.00}$	$O_{1.00}$	$O_{1.00}$	$O_{1.00}$
U_{eq}	0.0106(2)	0.0099(2)	0.0088(3)	0.0097(2)	0.0091(2)	0.0085(2)	0.0086(2)	0.0096(2)
O8								
x	0.20990(8)	0.20990(8)	0.2099(1)	−0.20985(7)	−0.20963(7)	0.20987(8)	−0.21008(9)	−0.20990(8)
y	0.27070(8)	0.27076(8)	0.2707(1)	−0.27070(7)	−0.27061(7)	0.27064(8)	−0.27078(9)	−0.27049(9)
z	0.4643(2)	0.4564(2)	0.4532(2)	−0.4656(1)	−0.46040(1)	0.45693(2)	−0.4585(2)	−0.4593(2)
occ.	$O_{1.00}$	$O_{1.00}$	$O_{1.00}$	$O_{1.00}$	$O_{1.00}$	$O_{1.00}$	$O_{1.00}$	$O_{1.00}$
U_{eq}	0.0122(2)	0.0111(2)	0.0106(3)	0.0113(2)	0.0101(2)	0.0101(2)	0.0102(2)	0.0108(2)

Definition for U_{eq} see Fischer & Tillmanns (1988).

Table 3. Selected interatomic distances (Å) in tourmalines from the Moldanubicum, Lower Austria.

		TK12	TK3	TK42	MASR	MAG	MAP12	BLG1	BLP1
X-	O2(x3)	2.513(2)	2.502(5)	2.480(5)	2.535(3)	2.492(2)	2.444(2)	2.451(2)	2.455(2)
	O5(x3)	2.762(2)	2.788(3)	2.787(3)	2.763(2)	2.753(2)	2.756(2)	2.755(2)	2.736(2)
	O4(x3)	2.817(2)	2.848(3)	2.852(3)	2.816(2)	2.818(2)	2.815(2)	2.813(2)	2.798(2)
Mean		2.697(2)	2.713(4)	2.706(4)	2.705(2)	2.688(2)	2.672(2)	2.673(2)	2.663(2)
Y-	O2(x2)	2.004(1)	1.976(1)	1.982(2)	1.990(1)	1.965(1)	1.974(1)	1.985(1)	1.971(1)
	O1(F1)	2.071(2)	2.020(3)	2.022(2)	2.035(2)	1.967(2)	2.032(2)	2.038(2)	2.004(2)
	O6(x2)	2.043(1)	2.030(1)	2.024(2)	2.034(1)	1.997(1)	2.023(1)	2.030(1)	1.999(1)
	O3	2.160(2)	2.128(2)	2.126(3)	2.155(2)	2.132(2)	2.156(2)	2.167(2)	2.150(2)
Mean		2.054(1)	2.027(2)	2.027(2)	2.040(2)	2.004(2)	2.030(2)	2.039(2)	2.016(2)
Z-	O6	1.865(1)	1.866(1)	1.865(2)	1.865(1)	1.865(1)	1.852(1)	1.850(1)	1.855(1)
	O7	1.883(1)	1.882(1)	1.887(2)	1.880(1)	1.8781(9)	1.882(1)	1.881(1)	1.883(1)
	O8	1.885(1)	1.883(1)	1.885(2)	1.885(1)	1.883(1)	1.881(1)	1.879(1)	1.877(1)
	O8	1.928(1)	1.922(1)	1.923(2)	1.925(1)	1.911(1)	1.912(1)	1.914(1)	1.905(1)
	O7	1.961(1)	1.955(1)	1.958(2)	1.957(1)	1.9417(9)	1.952(1)	1.955(1)	1.949(1)
	O3	1.9801(8)	1.9835(8)	1.981(1)	1.9829(7)	1.9744(7)	1.9634(8)	1.9646(9)	1.9584(9)
Mean		1.917(1)	1.915(1)	1.917(2)	1.916(1)	1.909(1)	1.907(1)	1.907(1)	1.905(1)
T-	O6	1.608(1)	1.608(1)	1.609(1)	1.6132(10)	1.6134(10)	1.602(1)	1.603(1)	1.600(1)
	O7	1.614(1)	1.613(1)	1.610(2)	1.6155(9)	1.6151(9)	1.612(1)	1.612(1)	1.605(1)
	O4	1.6259(6)	1.6213(6)	1.6222(8)	1.6249(5)	1.6220(5)	1.6229(6)	1.6241(7)	1.6179(7)
	O5	1.6409(7)	1.6341(7)	1.637(1)	1.6387(6)	1.6359(6)	1.6375(8)	1.6382(8)	1.6334(8)
Mean		1.622(1)	1.619(1)	1.620(1)	1.623(1)	1.622(1)	1.619(1)	1.619(1)	1.614(1)
B-	O2	1.359(3)	1.354(3)	1.360(4)	1.360(2)	1.360(2)	1.359(3)	1.361(3)	1.362(3)
	O8(x2)	1.383(2)	1.383(2)	1.381(2)	1.383(1)	1.380(1)	1.383(2)	1.384(2)	1.381(2)
Mean		1.375(2)	1.373(2)	1.374(3)	1.375(1)	1.373(1)	1.375(2)	1.376(2)	1.375(2)

Table 4. Chemical composition (wt%) of tourmalines from the Moldanubicum, Lower Austria.

	TK12	TK3	TK42	MASR	MAG	MAP12	BLG1	BLP1
SiO_2	33.90(15)	36.23(14)	36.20(22)	33.55(15)	34.82(23)	37.07(23)	35.82(21)	36.00(28)
TiO_2	0.97(2)	0.06(2)	0.06(2)	0.96(2)	0.09(1)	0.05(2)	0.31(10)	0.13(2)
Al_2O_3	32.82(17)	35.40(11)	34.59(28)	35.18(13)	40.33(19)	39.26(31)	37.38(53)	40.15(33)
B_2O_3	10.27(1)	10.43(2)	10.43	10.21(1)	11.40[2]	11.04(30)	10.82(8)	12.03(42)
FeO_{total}	13.15(10)	8.61(18)	8.75(13)	12.32(18)	5.02(16)	b. d.	4.05(42)	0.65(13)
FeO*	12.43	8.14	7.09	10.53	1.66	–	4.05	0.65
Fe_2O_3*	0.80	0.53	1.85	1.99	3.73	–	–	–
MnO	0.67(7)	0.59(5)	0.32(6)	0.77(5)	2.98(9)	4.83(30)	3.46(64)	3.17(33)
MgO	1.64(6)	3.33(9)	4.21(16)	0.77(3)	b. d.	b. d.	b. d.	b. d.
ZnO	0.04(4)	0.05(2)	0.04(1)	0.30(5)	0.27(4)	b. d.	0.04(2)	0.02(1)
CaO	0.28(3)	0.02(1)	0.03(1)	0.07(1)	0.06(1)	0.14(3)	0.31(5)	0.70(12)
Na_2O	2.29(6)	1.16(5)	1.53(7)	1.86(6)	1.81(9)	2.70(12)	2.80(7)	2.47(10)
K_2O	0.05(1)	b. d.	b. d.	0.04(1)	0.03(1)	0.02(1)	0.03(1)	b. d.
Li_2O	0.10(1)	0.03(1)	0.01	0.05(1)	0.32(3)	1.21(2)	0.90(7)	1.09(2)
H_2O	2.80	3.60[1]	3.57	3.33[1]	3.51[1]	2.99[1]	2.77(7)	3.13[1]
F	1.07(4)	0.09(3)	0.05(3)	0.49(2)	0.52(3)	1.60(20)	1.53(5)	1.37(9)
O≡F	−0.45	−0.04	−0.02	−0.21	−0.22	−0.67	−0.64	−0.58
Sum	99.68	99.62	99.96	99.89	101.31	100.24	99.58	100.33
N anions	31	31	31	31	31	31	31	31
Si	5.77	5.96	5.95	5.65	5.57	5.92	5.87	5.71
$^{[4]}$Al	0.21	0.04	0.05	0.35	0.28	0.04	0.07	–
$^{[4]}$B	0.02	–	–	–	0.15	0.04	0.06	0.29
Sum *T* site	6.00	6.00	6.00	6.00	6.00	6.00	6.00	6.00
$^{[3]}$B	3.00	2.96	2.96	2.97	3.00	3.00	3.00	3.00
Al	6.38	6.83	6.65	6.63	7.32	7.35	7.15	7.50
Mn^{2+}	0.10	0.08	0.04	0.11	0.40	0.65	0.48	0.43
Fe^{2+}	1.77	1.12	0.97	1.48	0.22	–	0.56	0.09
Fe^{3+}	0.10	0.07	0.23	0.25	0.45	–	–	–
Mg	0.42	0.82	1.03	0.19	–	–	–	–
Zn	0.01	0.01	–	0.04	0.03	–	0.01	–
Ti^{4+}	0.12	0.01	0.01	0.12	0.01	0.01	0.04	0.02
Li	0.07	0.02	0.01	0.03	0.21	0.78	0.59	0.69
Sum *Y*, *Z* sites	8.97	8.96	8.94	8.85	8.64	8.79	8.83	8.73
Ca	0.05	–	–	0.01	0.01	0.02	0.05	0.12
Na	0.76	0.37	0.49	0.61	0.56	0.84	0.89	0.76
K	0.01	–	–	0.01	0.01	–	0.01	–
□	0.18	0.63	0.51	0.37	0.42	0.14	0.05	0.12
Sum *X* site	1.00	1.00	1.00	1.00	1.00	1.00	1.00	1.00
Sum cations	18.79	18.29	18.39	18.45	18.22	18.65	18.78	18.61
OH	3.18	3.95	3.91	3.74	3.74	3.19	3.03	3.31
F	0.58	0.05	0.03	0.26	0.26	0.81	0.79	0.69
Sum OH + F	3.76	4.00	3.94	4.00	4.00	4.00	3.82	4.00

Note: Samples TK12, TK3, and TK42 are from Königsalm; samples MASR, MAG, MAP12 are from Maigen; samples BLG1 and BLP1 are from Blocherleitengraben. TK12: average of 16 EMP analyses; B_2O_3, Li_2O and Be (8 ppm) from 2 SIMS analyses; H_2O, 1 SIMS analysis. TK3: average of 14 EMP analyses; B_2O_3, Li_2O, H_2O and Be (1 ppm) from 3 SIMS analyses. TK42: average of 5 EMP analyses; B_2O_3, Li_2O, H_2O and Be (1 ppm) from 1 SIMS analysis. MASR: average of 18 EMP analyses; B_2O_3, Li_2O, H_2O and Be (7 ppm) from 3 SIMS analyses. MAG: average of 10 EMP analyses; B_2O_3 (10.53(4) wt%), Li_2O, H_2O and Be (5 ppm) from 2 SIMS analyses. MAP12: average of 14 EMP analyses; B_2O_3, Li_2O and Be (13 ppm) from 2 SIMS analyses; H_2O, 1 SIMS analysis. BLG1: average of 18 EMP analyses; B_2O_3, Li_2O, H_2O and Be (6 ppm) from 3 SIMS analyses. BLP1: average of 12 EMP analyses; B_2O_3, Li_2O and Be (5 ppm) from 2 SIMS analyses; H_2O, 1 SIMS analysis. Cl and Cr are below detection limit. b. d. = below detection limit. *FeO and Fe_2O_3 were calculated on basis of the Mössbauer spectra, except samples TK42, MAG, BLP1 and BLG1 (calculated on basis of the <*Y*-O> distances; see Table 3 and text). Mn was generally calculated as MnO, although small amounts of Mn^{3+} will occur because of the pink colour of some samples (see text). [1]H_2O was calculated for (OH) + F = 4.00. SIMS data for H_2O: MASR, 3.46(5) wt%; TK3, 3.66(10) wt%; MAG, 3.57(2); MAP12, 3.14 wt%; BLP1, 3.24 wt%. The H_2O value of TK3 and TK42 was also determined by TGA (3.58 wt%) on a bulk analysis of the whole crystal (TK3 and TK42). [2]B_2O_3 calculated with the procedure (formula for the calculation of the *T*-site occupants) described by Ertl *et al.* (2007).

3.4. Sm-Nd isotope analysis

Garnet (50–100 mg) and plagioclase (100–250 mg) used for isotope analyses were hand-picked under a binocular microscope from defined sieve (0.20–0.30 mm) and magnetic fractions. For monazite and xenotime, single crystals, each about 10 mg in weight, were used. To remove surface contaminants, all fractions were washed in acetone and

water before decomposition. Additionally, garnet was leached in 2.5 N HCl at *ca*. 80 °C for 30 min. Chemical sample preparation for Sm–Nd isotope analyses was performed at the Geological Survey of Austria, following the procedure described by Sölva *et al.* (2005). The measurements of the isotopic ratios were performed at the Department of Lithospheric Research at the Universität Wien. Spiked Sm and Nd ratios were determined on a Finnigan® MAT 262 magnetic sector thermal ionisation mass spectrometer (TIMS), whereas unspiked Nd ratios were analysed on a ThermoFinnigan® Triton TI TIMS. Overall blank contributions were $\leq$ 0.2 ng for Nd and Sm. All elements were run from Re double filaments. During the period of measurements the La Jolla standard yielded $^{143}Nd/^{144}Nd = 0.511845 \pm 1$ ($n = 12$) on the Triton TI. Errors for the $^{147}Sm/^{144}Nd$ ratio are ± 2 % or smaller, as determined on the basis of iterative sample analysis and spike recalibration. Isochron ages were calculated with the software ISOPLOT/Ex (Ludwig, 2003).

Monazite and xenotime chemical analyses were performed on a Jeol JX 8600 microprobe following the routine established at the Abteilung Mineralogie, Universität Salzburg. The routine involves a complete wavelength dispersive (WD) analysis for elements Si, P, La, Ce, Pr, Nd, Sm, Gd, Dy, Er, Yb, Y, Th, U, Ca and Pb. A detailed description of standards, element lines, counting times, background positions, background, and interference corrections used in the Salzburg microprobe laboratory for monazite and xenotime analysis is given in Krenn *et al.* (2008). Chemical Th-U-Pb ages for monazite were calculated following the method of Montel *et al.* (1996) (Table S4). The analytical errors of a point analysis typically correspond to a ~10–30 Ma error on the age (1 σ). A weighted average age with reduced error can be calculated from a larger number of measurements in coherent age domains.

3.5. U-Pb laser-ablation MC-ICP-MS analysis

Six fragments of large monazite crystals were mounted in a one-inch epoxy resin disk, ground, and polished to thin-section quality. Internal structures were revealed using back-scattered electron imaging using a Jeol 6400 SEM at the Department of Lithospheric Research, University of Vienna. These images were used to select homogeneous parts of crystals suitable for laser-ablation MC-ICP-MS dating and to detect mineral zonation, inclusions and other impurities. Monazite *in situ* $^{206}Pb/^{238}U$ and $^{207}Pb/^{206}Pb$ ages were determined using a 193 nm solid-state Nd-YAG laser (NewWave UP193-SS) coupled to a multi-collector ICP-MS (Nu Instruments HR). Ablation in a He atmosphere was raster-wise, avoiding any imperfections of the crystal according to BSE zonation patterns. Line width for rastering was 5 μm with a rastering speed of 5 μm/s and a raster length of 50 μm. Energy densities were 5–8 J/cm^2 with a repetition rate of 10 Hz. Ablation duration was 20–50 s with a 40 s gas and Hg blank measurement immediately preceding ablation. Mass bias and mass fractionation corrections were made using an in-house monazite standard (Rastenberg RGB; Friedl *et al*., 1993). The standard monazite was also used as a secondary standard during the course of the analytical session. The overall accuracy and precision for the method derived from these measurements are 2 % and 1 %, respectively (2RSD, 15 measurements). For more analytical details, see Klötzli *et al.* (2009). Final statistics and age calculations were made using Isoplot (Ludwig, 2003) (A table of these data is available from the GSW website or from the first author). Errors shown are all at the 2-σ level.

3.6. Mössbauer analysis

Approximately 30 mg of each tourmaline (samples TG12 and MASR) were crushed to a fine powder under acetone and mixed with sugar before mounting in a sample holder confined by Kapton® polyimide film tape. The resultant sample thicknesses were well below the thin absorber thickness approximation of Long *et al.* (1983). Room-temperature Mössbauer spectra were acquired to determine Fe^{2+} and Fe^{3+} content in the Mineral Spectroscopy Laboratory at Mount Holyoke College. A source of ~50 mCi ^{57}Co in Rh was used on a WEB Research Co. spectrometer. Run time for each spectrum was ~48 h. Results were calibrated against α-Fe foil of 6 μm thickness and 99 % purity. In the absence of *any* data on recoil-free fractions for Fe in different sites and valences in the tourmaline structure, peak areas were assumed to correspond directly to the abundance of the species in the sample. The error on $\%Fe^{3+}$ in these samples is estimated at ±1–3 % absolute. The error on site assignments (*i.e.*, on the distribution of areas among sub-distributions of Fe on a single site, such as $^{[Y]}Fe^{2+}$) is approximately ±5–15 %. Spectra were processed using the DIST_3D program, an implementation of software described in Wivel & Mørup (1981). The program uses quadrupole splitting distributions with Lorentzian lineshapes and an assumed average correlation between the isomer shift and quadrupole shift in each of two valence states. Widths, isomer shifts and quadrupole splittings of the doublets were allowed to vary. Errors on isomer shift and quadrupole splitting of well-resolved peaks are usually ±0.02 mm/s. However, this spectrum could only be fit with a combination of heavily overlapping doublets (Fig. 2), so the errors are probably ±0.05–0.1 mm/s.

3.7. Optical absorption spectra

Polarised optical absorption spectra (Fig. 3) in the 380–1700 nm range were obtained at about 1.5 nm resolution with a microspectrometer system consisting of diode-array detectors coupled to a grating spectrometer system *via* fibre optics to a highly modified NicPlan® infrared microscope containing a calcite polarizer. A pair of conventional 10× objectives was used as an objective and a condenser. In the 380–1050 nm range, a 1024-element Si array was used, and in the 1050–1700 nm range, a 256-element InGaAs array was employed.

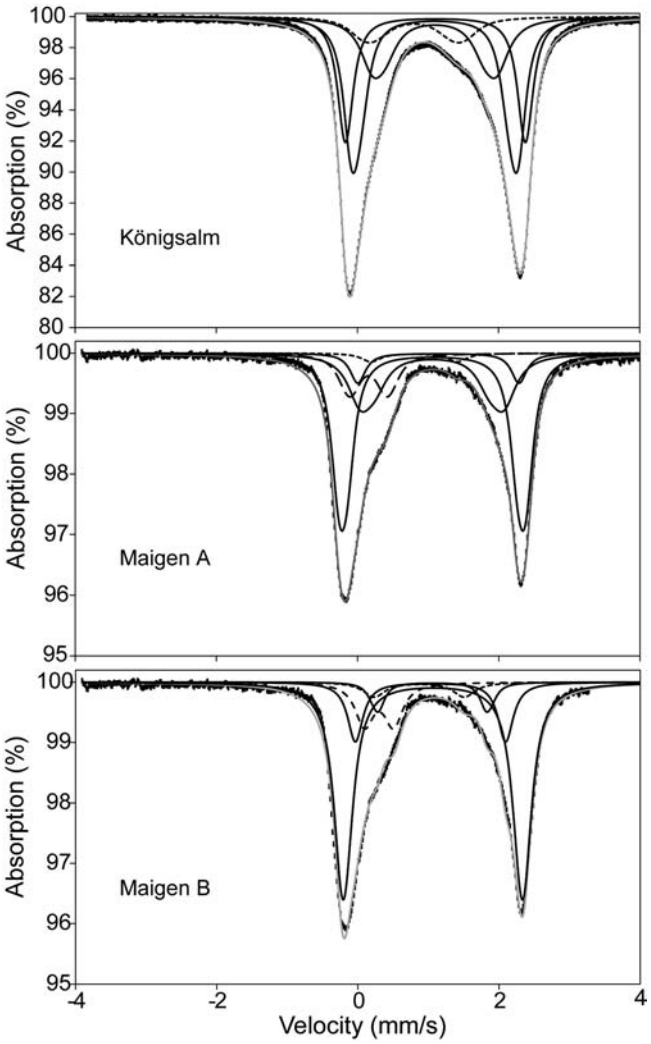

Fig. 2. Room-temperature Mössbauer spectra of the Königsalm (TK12) and Maigen (MASR) samples. Data points are plotted as error bars and the fit envelope is a solid gray line. Fe^{2+} distributions are shown as solid black lines, the ED feature as dotted lines, and the Fe^{3+} distribution as a dashed line. The lower two plots are fits to the same spectrum with slightly different parameters (see discussion in text and Table S5).

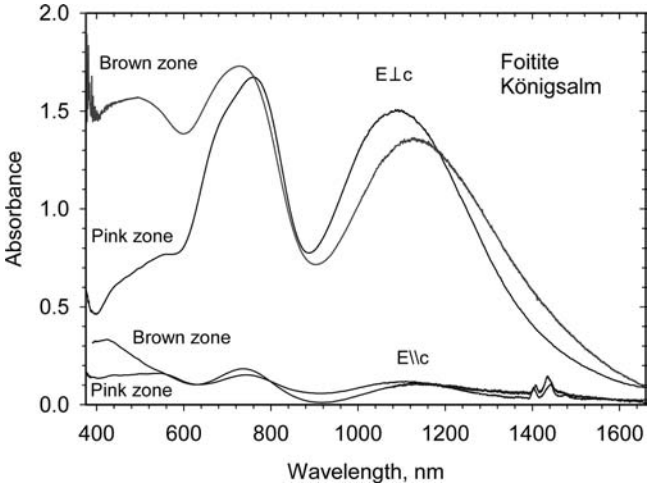

Fig. 3. Optical absorption spectra of foitite (pink zone = sample TK3; the brown zone is found right to the pink zone of the crystal shown in Fig. 4) from Königsalm, Lower Austria.

4. Results

4.1. Mineral compositions

4.1.1. Pegmatite Königsalm

Thin prismatic crystals (a few hundred μm in diameter) of black-to-brown tourmaline (TK12, Fig. 4), which occur together with idioblastic albite in tiny pockets, are classified as fluor-schorl, with the relatively homogeneous composition $\sim^{X}(Na_{0.8}Ca_{0.1}\square_{0.2})$ $^{Y}(Fe^{2+}{}_{1.8}Al_{0.6}Mg_{0.2}Ti^{4+}{}_{0.1}Mn^{2+}{}_{0.1}Li_{0.1})$ $^{Z}(Al_{5.8}Mg_{0.2})$ $(BO_3)_3$ $[Si_{5.8}Al_{0.2}O_{18}]$ $^{V}(OH)_3$ $^{W}[F_{0.6}O_{0.2}(OH)_{0.2}]$ and lattice parameters a = 15.987(2), c = 7.163(2) Å (Tables 1 and 4; detailed site occupancies of all tourmalines in Table 5). The assignment of the *Z*-site occupation is discussed below. Large black schorl crystals (up to ~10 cm in length), intergrown with feldspar and quartz, have similar lattice parameters (a = 15.993(2), c = 7.169(2) Å). Tourmaline crystals with pink (TK3, Fig. 4) and greenish-gray (TK42, Fig. 4) coloured zones can be classified as foitite and magnesiofoitite, respectively. Analyses of the relatively homogeneous cross-sections yield chemical formulae $\sim^{X}(\square_{0.6}Na_{0.4})$ $^{Y}(Fe^{2+}{}_{1.1}Al_{1.1}Mg_{0.6}Mn^{2+}{}_{0.1}Fe^{3+}{}_{0.1})$ $^{Z}(Al_{5.7}Mg_{0.3})$ $(BO_3)_3$ $[Si_6O_{18}]$ $^{V}(OH)_3$ $^{W}[(OH)_{0.9}F_{0.1}]$ (TK3) and $^{X}(\square_{0.5}Na_{0.5})$ $^{Y}(Fe^{2+}{}_{1.0}Al_{0.9}Mg_{0.8}Fe^{3+}{}_{0.2}\square_{0.1})$ $^{Z}(Al_{5.7}Mg_{0.3})$ $(BO_3)_3$ $[Si_{5.9}Al_{0.1}O_{18}]$ $^{V}(OH)_3$ $^{W}[(OH)_{0.9}O_{0.1}]$ (TK42) (Tables 4 and 5). Dark-reddish-orange-coloured garnet (Grt1, up to ~8 mm in diameter, Table S2, Fig. 5), which has 53 mol% spessartine, 46 mol% almandine and 1 mol% pyrope, is associated with pure albite and muscovite, up to ~3 cm in diameter (Fsp1, Table S2, Fig. 5; M1, Table S3). In the zones where the large biotite plates are associated with muscovite and perthitic feldspar, biotite has the formula $K(Fe^{2+}{}_{1.7}Mg_{0.6}Al_{0.5}Ti^{4+}{}_{0.2})[AlSi_3O_{10}](OH)_2$ and contains 57 mol% annite (M3, Table S3, Fig. 5). Feldspar consists of a K-feldspar host with 85 mol% microcline, 13 mol% albite and 2 mol% anorthite (Fsp3; Table S2, Fig. 5) and albite exsolution lamellae (with 1 mol% anorthite and 1 mol% K-feldspar; Fsp4, Table S2). Associated muscovite (crystals up to ~5 mm wide) has a composition of $(K_{0.9}Na_{0.1})(Al_{1.8}Fe^{2+}{}_{0.1}Mg_{0.1})[AlSi_3O_{10}](OH)_2$ (M2, Table S3, Fig. 5). Monazite-(Ce) is relatively homogeneous and has an average composition of $\sim(Ce_{0.4}La_{0.2}\,Nd_{0.1}Y_{0.1}Th_{0.1}Ca_{0.1})_{\sum 1.0}\,[PO_4]$ (Table S4, Fig. 5). The xenotime-(Y) crystals show a weak zoning, close to $\sim(Y_{0.7}Dy_{0.1}Yb_{0.1}Er_{0.1})_{\sum 1.0}\,[PO_4]$ in composition (Table S5). Xenotime consists of 75 mol% xenotime-(Y) and 5–7 mol% xenotime-(Yb) (Table S5). Additionally, pale-brown short prismatic crystals, up to ~100 μm in size, found in a tiny pocket, were identified as allanite-(Ce) with a = 8.893(1), b = 5.699(1), c = 10.116(1) Å, β = 114.91(1)°.

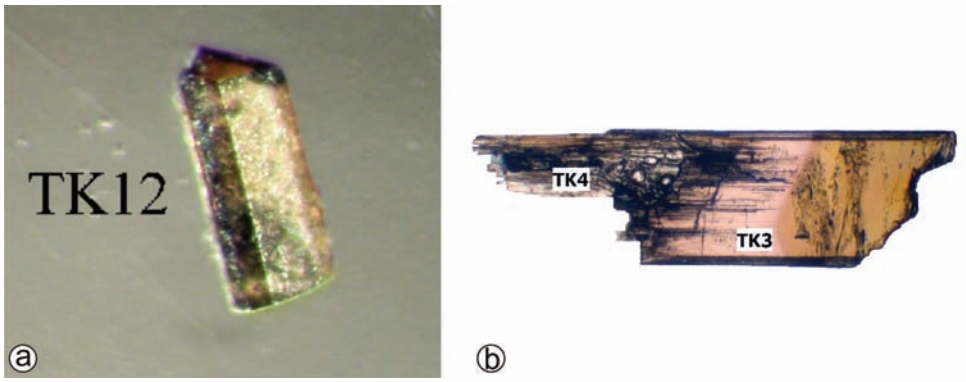

Fig. 4. Coloured tourmalines from the Königsalm pegmatite (Moldanubian nappes, Lower Austria). (a) Brownish fluor-schorl (sample TK12) with ~300 μm in length, (b) Pink foitite (TK3) and greenish-gray magnesiofoitite (TK42).

Table 5. Site occupancies in tourmalines from the Moldanubicum, Lower Austria

Sample	*X* site	*Y* site	*Z* site	*T* site	*W* site
TK12	$Na_{0.76}Ca_{0.05}K_{0.01}\square_{0.18}$	$Fe^{2+}_{1.77}Al_{0.62}Mg_{0.19}Ti^{4+}_{0.12}Mn^{2+}_{0.10}Fe^{3+}_{0.09}Li_{0.07}Zn_{0.01}\square_{0.03}$	$Al_{5.76}Mg_{0.23}Fe^{3+}_{0.01}$	$Si_{5.77}Al_{0.21}B_{0.02}$	$F_{0.58}O_{0.24}(OH)_{0.18}$
TK3	$\square_{0.63}Na_{0.37}$	$Fe^{2+}_{1.12}Al_{1.09}Mg_{0.56}Mn^{2+}_{0.08}Fe^{3+}_{0.07}Li_{0.02}Ti^{4+}_{0.01}Zn_{0.01}\square_{0.04}$	$Al_{5.74}Mg_{0.26}$	$Si_{5.96}Al_{0.04}$	$(OH)_{0.95}F_{0.05}$
TK42	$\square_{0.51}Na_{0.49}$	$Fe^{2+}_{0.97}Al_{0.93}Mg_{0.75}Fe^{3+}_{0.23}Mn^{2+}_{0.04}Li_{0.01}Ti^{4+}_{0.01}\square_{0.06}$	$Al_{5.72}Mg_{0.28}$	$Si_{5.95}Al_{0.05}$	$(OH)_{0.91}O_{0.06}F_{0.03}$
MASR	$Na_{0.61}\square_{0.37}Ca_{0.01}K_{0.01}$	$Fe^{2+}_{1.48}Al_{0.89}Mg_{0.13}Ti^{4+}_{0.12}Mn^{2+}_{0.11}Fe^{3+}_{0.05}Zn_{0.04}Li_{0.03}\square_{0.15}$	$Al_{5.74}Fe^{3+}_{0.20}Mg_{0.06}$	$Si_{5.65}Al_{0.35}$	$(OH)_{0.74}F_{0.26}$
MAG	$Na_{0.56}\square_{0.42}Ca_{0.01}K_{0.01}$	$Al_{1.32}Fe^{3+}_{0.45}Mn^{2+}_{0.40}Fe^{2+}_{0.22}Li_{0.21}Zn_{0.03}Ti^{4+}_{0.01}\square_{0.36}$	Al_6	$Si_{5.57}Al_{0.28}B_{0.15}$	$(OH)_{0.74}F_{0.26}$
MAP12	$Na_{0.84}\square_{0.14}Ca_{0.02}$	$Al_{1.35}Li_{0.78}Mn^{2+}_{0.65}Ti^{4+}_{0.01}\square_{0.21}$	Al_6	$Si_{5.92}Al_{0.04}B_{0.04}$	$F_{0.81}(OH)_{0.19}$
BLG1	$Na_{0.89}Ca_{0.05}\square_{0.05}K_{0.01}$	$Al_{1.15}Li_{0.59}Fe^{2+}_{0.56}Mn^{2+}_{0.48}Ti^{4+}_{0.04}Zn_{0.01}\square_{0.17}$	Al_6	$Si_{5.87}Al_{0.07}B_{0.06}$	$F_{0.79}O_{0.18}(OH)_{0.03}$
BLP1	$Na_{0.76}Ca_{0.12}\square_{0.12}$	$Al_{1.52}Li_{0.69}Mn^{2+}_{0.43}Fe^{2+}_{0.09}\square_{0.27}$	$Al_{5.98}Ti^{4+}_{0.02}$	$Si_{5.71}B_{0.29}$	$F_{0.69}(OH)_{0.31}$

Note: The *V* site is in all samples occupied with $(OH)_3$, and the *B* site with $\sim B_3$ (details see Table 4). There is no clear evidence for small amounts of Ti^{4+} at the *Z* site of sample BLP1.

4.1.2. Pegmatite Maigen

Black, short-prismatic, relatively homogeneous tourmaline (MASR) from small pockets are schorl with formula $\sim{}^{X}(Na_{0.6}\square_{0.4})\ {}^{Y}(Fe^{2+}_{1.5}Al_{0.9}Mg_{0.1}Ti^{4+}_{0.1}Mn^{2+}_{0.1}Fe^{3+}_{0.1}\square_{0.2})\ {}^{Z}(Al_{5.7}Fe^{3+}_{0.2}Mg_{0.1})\ (BO_3)_3\ [Si_{5.7}Al_{0.3}O_{18}]\ {}^{V}(OH)_3\ {}^{W}[(OH)_{0.7}F_{0.3}]$ (Tables 4 and 5). Pale-pink (MAP12) and dark-green (MAG) tourmaline crystals are classified as Mn-bearing ''fluor-elbaite'', respectively Fe-, Mn- and Li-bearing olenite with the crystal chemical formulae $\sim{}^{X}(Na_{0.9}\square_{0.1})\ {}^{Y}(Al_{1.3}Li_{0.8}Mn^{2+}_{0.7}\square_{0.2})\ {}^{Z}Al_6\ (BO_3)_3\ [Si_{5.9}Al_{0.1}O_{18}]\ {}^{V}(OH)_3\ {}^{W}[F_{0.8}(OH)_{0.2}]$ (MAP12) and $\sim{}^{X}(Na_{0.6}\square_{0.4})\ {}^{Y}(Al_{1.3}Fe^{3+}_{0.5}Mn^{2+}_{0.4}Fe^{2+}_{0.2}Li_{0.2}\square_{0.4})\ {}^{Z}Al_6\ (BO_3)_3\ [Si_{5.6}Al_{0.3}B_{0.1}O_{18}]\ {}^{V}(OH)_3\ {}^{W}[(OH)_{0.7}F_{0.3}]$ (MAG) (Tables 4 and 5). Pale-pink ''fluor-elbaite'' is intergrown with albite with 1 mol% anorthite (Fsp5, Table S2, Fig. 6) and microcline (Fsp6, Table S2, Fig. 6). Reddish-brown garnet (Grt2, up to ~5 mm in diameter, Table S2, Fig. 6), which has 56 mol% almandine, 36 mol% spessartine, 7 mol% pyrope and 1 mol% grossular, is associated with plagioclase An_8 (Fsp2, Table S2, Fig. 6).

4.1.3. Pegmatite Blocherleitengraben

The pink-coloured rim (BLP1) of a multicoloured tourmaline crystal (from a small pocket) is identified as a Mn-bearing, B-rich ''fluor-elbaite'' with formula $\sim{}^{X}(Na_{0.8}Ca_{0.1}\square_{0.1})\ {}^{Y}(Al_{1.5}Li_{0.7}Mn^{2+}_{0.4}Fe^{2+}_{0.1}\square_{0.3})\ {}^{Z}Al_6\ (BO_3)_3\ [Si_{5.7}B_{0.3}O_{18}]\ {}^{V}(OH)_3\ {}^{W}[F_{0.7}(OH)_{0.3}]$ (Table 4). A greenish-brown zone (BLG1), rimming schorl, is classified as a Fe- and Mn-bearing ''fluor-elbaite'' with formula $\sim{}^{X}(Na_{0.9}Ca_{0.1})\ {}^{Y}(Al_{1.1}Li_{0.6}Fe^{2+}_{0.6}Mn^{2+}_{0.5}\square_{0.2})\ {}^{Z}Al_6\ (BO_3)_3\ [Si_{5.9}Al_{0.1}O_{18}]\ {}^{V}(OH)_3\ {}^{W}[F_{0.8}O_{0.2}]$ (Tables 4 and 5).

4.2. Mössbauer analysis of tourmalines

Resultant parameters of fits of Mössbauer spectra (Table 6; Fig. 2) are in general agreement with those reported in Dyar *et al.* (1998). The first three doublets have parameters matching those for Fe^{2+} at the *Y* site. The fourth doublet, which has an isomer shift of 0.80 mm/s in both spectra, lies in the range for electron-delocalised peaks, which

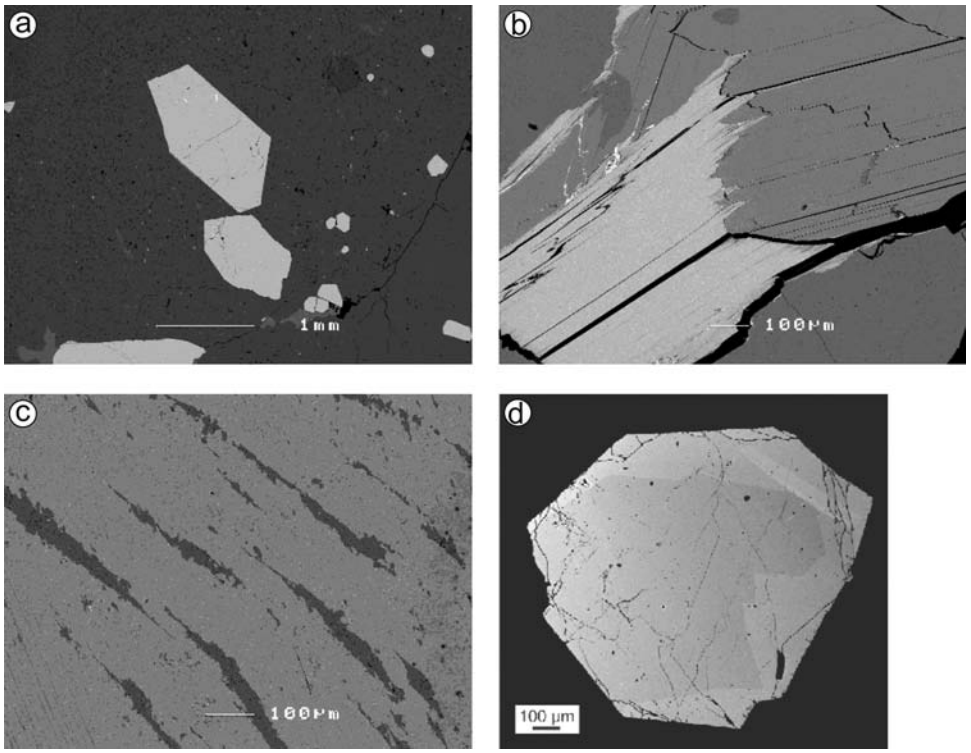

Fig. 5. Back-scattered electron images of samples from the pegmatite from Königsalm (Moldanubian nappes, Lower Austria). (a) Spessartine-almandine crystals (light gray) in albite (dark gray), samples from domains of coarse-grained biotite intergrown with feldspar (Sample EK2): (b) ''Biotite'' (annite), intergrown with muscovite, (c) Perthite (microcline host with albite exsolution lamellae), (d) zoned monazite-(Ce) crystal.

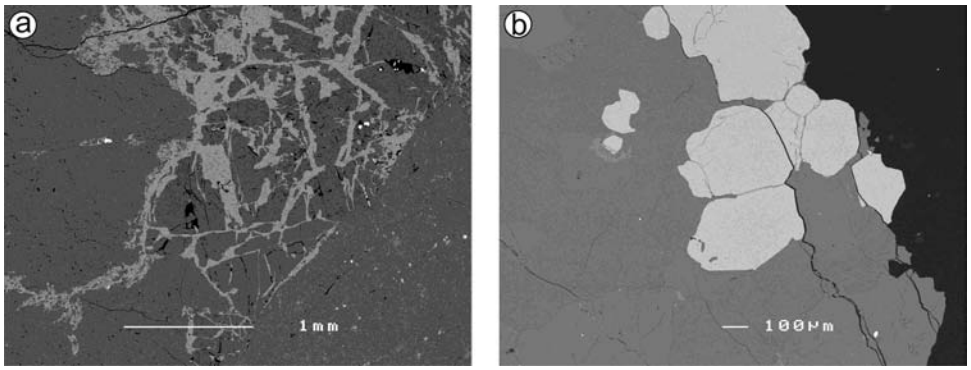

Fig. 6. Back-scattered electron images of samples from the pegmatite from Maigen (Moldanubian nappes, Lower Austria). (a) Fragmented pale-pink elbaite (dark grey) intergrown with albite and microcline (light grey), (b) Almandine-spessartine crystals (light grey) in plagioclase (dark grey) (sample EM1).

represent sharing of an electron between Fe^{2+} and Fe^{3+}. Thus, the area of this doublet must be split between the two valence states. From these data, we can conclude that the Königsalm sample (TK12) contains $\sim$5 % Fe^{3+}.

The fifth distribution (in the Maigen sample MASR only) was fit in two ways. A completely unconstrained fit yields a doublet with parameters of isomer shift equal to 0.16 mm/s and quadrupole splitting of 0.50 mm/s – listed as ''Maigen A'' in Table 6. Although this fit is better numerically ($\chi^2 = 3.145$), these are parameters usually associated with tetrahedral Fe^{3+} in silicates and the structure refinement gives unequivocal support for the occupancy of Fe^{3+} in the Z site. Thus the fit was repeated using constraints on the minimum isomer shift, resulting in the ''Maigen B'' parameters given in Table 6, with an isomer shift of 0.30 mm/s that is more appropriate for Fe^{3+} in octahedral coordination. The latter fit results in a higher (worse) χ^2 value of 5.395, and the slight misfit of this model is apparent in Fig. 4. The tetrahedral-like parameters for this doublet may suggest that the octahedron is distorted, with the Fe^{3+} displaced off-centre, enough so it ''feels'' the effect of only the four closest oxygens in the

Table 6. Mössbauer parameters of tourmalines from Königsalm and Maigen, Lower Austria.

Assignment	Parameter	Königsalm	Maigen A	Maigen B
Y-site Fe^{2+}	δ, mm/s	1.11	1.06	1.06
	Δ, mm/s	2.55	2.65	2.57
	Γ, mm/s	0.25	0.25	0.29
	%Area	26	51	62
Y-site Fe^{2+}	δ, mm/s	1.10	1.15	1.03
	Δ, mm/s	2.38	2.27	2.13
	Γ, mm/s	0.25	0.25	0.26
	%Area	39	7	15
Y-site Fe^{2+}	δ, mm/s	1.10	1.06	1.06
	Δ, mm/s	1.77	2.03	1.52
	Γ, mm/s	0.40	0.40	0.22
	%Area	23	27	6
Fe^{2+}–Fe^{3+} ED	δ, mm/s	0.80	0.80	0.87
	Δ, mm/s	1.17	1.24	1.28
	Γ, mm/s	0.44	0.32	0.38
	%Area	11	3	5
Octahedral Fe^{3+}	δ, mm/s		0.16	0.30
	Δ, mm/s		0.50	0.40
	Γ, mm/s		0.30	0.30
	%Area		13	12
	χ^2	4.100	3.145	5.395
	Total %Fe^{3+}	5.5 %	14.5 %	14.5 %

Note: Results are given in mm/s relative to the centre point of a Fe foil calibration spectrum. Γ = the Lorentzian peak-width at half-maximum. Errors on isomer shift (δ) and quadrupole splitting (Δ) are discussed in the text. ED = delocalised electrons.

octahedron. Both fits result in the same Fe^{3+} content for the Maigen sample overall: ∼14 % Fe^{3+}.

4.3. Colour and optical absorption spectra of tourmalines

The optical absorption spectrum of the pink foitite (TK3) from the Königsalm pegmatite shows strong dichroism with the maximum intensity in the **E**⊥*c* direction. The spectrum consists of sharp OH bands near 1400 nm in **E**//*c*, Fe^{2+} bands in both polarisations at about 1100 and 750 nm, and a Fe^{2+}-Ti^{4+} intervalence charge transfer at about 440 nm (Smith, 1977; Mattson & Rossman, 1988). The Mn^{3+} absorption that occurs at 515 nm is apparent in elbaite (Reinitz & Rossman, 1988), but poorly resolved in this region in the foitite spectrum. The striking difference in intensity between the **E**⊥*c* and **E**//*c* directions is due to the interaction of Fe^{3+} with the Fe^{2+} (Mattson & Rossman, 1987). This interaction dramatically increases the intensity of the Fe^{2+} absorption in the **E**⊥*c* direction. The striking dichroism between blue and pink in region TK3 occurs because the intensified Fe^{2+} bands in the **E**⊥*c* direction confine most of the transmitted light to the blue portion of the spectrum, whereas in the **E**//*c* direction, the maximum transmission occurs in the 630 nm region (a weak bias towards the red portion of the spectrum). When viewed in polarised light in the **E**⊥*c* direction, region TK3 shows an inhomogeneous distribution of blue colour suggesting that the proportion of Fe^{3+} is not uni- form. Nevertheless, an estimate of the amount of Fe^{3+} in the tourmaline can be obtained using Fig. 6 of Mattson & Rossman (1987) which shows the difference between the intensity of the Fe^{2+} bands in the two polarisations. Although not a rigorous calibration, the figure suggests that, in the region of the foitite where the optical spectrum was taken, about 3 % of the Fe^{2+} is interacting with Fe^{3+}. Using the 8.14 wt% FeO value and the calculated density of 3.12, this suggests that about 2.5 % of the iron is Fe^{3+}, a value of similar magnitude to the average Fe^{3+} proportion determined by the Mossbauer data of 5.5 %. The absorption spectrum also explains the dark colour of the tip of the crystal (brown region near the pink region of the crystal shown in Fig. 4) in the E⊥*c* direction. Here, the transmission of light in the blue region of the spectrum is blocked by absorption from the Fe^{2+}-Ti^{4+} interaction whereas the light in the longer-wavelength region is blocked by absorption from the Fe^{2+}-Fe^{3+} interaction.

4.4. Geochronology and isotope geology

To determine the ages of the pegmatites, Sm-Nd analyses were performed on feldspar (EK1 Fsp), garnet (EK1 Grt), monazite (EK2 Mnz) and xenotime (EK2 Xen) from the Königsalm locality; from Maigen, albite (EM Fsp) and garnet (EM Grt) were analysed (Table 7). Additionally, a chemical U-Th-Pb age was determined on monazite of sample EK2 (Table S4) from the Königsalm pegmatite.

Feldspars of sample EK1 are characterised by very low Nd (0.024 ppm) and Sm (0.007 ppm) concentrations and a low $^{147}Sm/^{144}Nd$ ratio of 0.1685, which is typical for feldspar. The garnet displays higher concentrations in Nd

Table 7. Sm-Nd isotopic data for samples from the Königsalm (EK1, EK2) and Maigen (EM1) pegmatite, from the Moldanubian nappes in Lower Austria.

Sample	Nd (ppm)	Sm (ppm)	$^{147}Sm/^{144}Nd$	$^{143}Nd/^{144}Nd$	2σ (m)
EK1 Fspl	0.024	0.007	0.1685	0.512315	1.5E-05
EK1 Grt1	2.443	2.593	3.5422	0.519692	3.5E-06
EK2 Xen	3363	4695	0.8443	0.513787	5.2E-06
EK2 Mnz	96493	19585	0.1227	0.512229	2.4E-06
EM1 Fsp2	0.317	0.076	0.1454	0.512331	8.4E-06
EM1 Grt2	0.191	1.521	4.8356	0.522749	1.8E-05

Note: Abbreviations: Grt = garnet, Fsp = feldspar, Mnz = monazite, Xen = xenotime.

(0.443 ppm) and Sm (2.593 ppm) and it is highly enriched in the heavy REE as also shown by the high $^{147}Sm/^{144}Nd$ ratio of 3.542. The calculated isochron age for the two data points is 334 ± 4 Ma and the initial $^{143}Nd/^{144}Nd$ ratio is 0.511946 ± 16, corresponding to an $\varepsilon_{Nd(t\,=\,334\ Ma)}$ of –5.1. The Nd and Sm concentrations of monazite and xenotime of sample EK2 (Table 7) are in a similar range to the electron microprobe results (Tables S4 and S5). Monazite shows the higher concentrations, it is enriched in the LREE, and has a $^{147}Sm/^{144}Nd$ ratio of 0.1227, whereas xenotime is enriched in the HREE and is characterised by a $^{147}Sm/^{144}Nd$ ratio of 0.8443. This allows calculation of a 330 ± 4 Ma isochron age for sample EK2 also. The initial $^{143}Nd/^{144}Nd$ ratio is 0.511964 ± 5 and corresponds to a $\varepsilon_{Nd(t\,=\,330\ Ma)}$ of –4.9. Calculation of an isochron including the minerals from both samples yields an age of 332 ± 3 Ma (Fig. 7a). *In situ* laser-ablation U-Pb ages (62 values) on six different monazite crystal fragments are all concordant and identical within the assigned errors. The concordia age, calculated for all points, is 330 ± 4 Ma (Fig. 7c).

A Th* *versus* Pb isochron diagram for monazite of sample EK2 is given in Fig. 7d. It is based on the analyses in Table S4 and defines a model isochron with a weighted average age of 334 ± 14 Ma. The model isochron calculated from the xenotime analyses with the highest Th and U contents yields a poorly constrained age (345 ± 26 Ma) that fits the age of the monazite.

Additionally, in the pegmatite from Maigen, the feldspar shows low Nd and Sm concentrations and a $^{147}Sm/^{144}Nd$ ratio of 0.1454, which is similar to feldspar in the Königsalm pegmatite. The garnet is characterised by even lower Nd and Sm concentrations and a more pronounced enrichment in the HREE ($^{147}Sm/^{144}Nd = 4.836$) than the garnet from the Königsalm pegmatite. On the basis of the two data points, the isochron age is 339 ± 4 Ma at an initial $^{143}Nd/^{144}Nd$ ratio is 0.512008 ± 10 the ($\varepsilon_{Nd(t\,=\,339\ Ma)}$ is –3.8) (Fig. 7b).

5. Discussion

5.1. Tourmalines, crystal structure, chemistry and correlations

Several efforts have been made to address the Mg-Al disordering between the *Y* and *Z* site in the tourmaline atomic arrangement (Grice & Ercit, 1993; Hawthorne *et al*., 1993; Bloodaxe *et al*., 1999; Ertl *et al*., 2003b; Bosi & Lucchesi, 2004, 2007). These authors demonstrated that Mg and Fe^{3+} not only occupy the *Y* site but also the *Z* site in tourmaline. However, in many cases it is problematic to assign the cations in a way that the average ionic radius of the *Y*-site occupants fits the <*Y*-O> bond length while the average ionic radius of the *Z*-site occupants simultaneously fits the

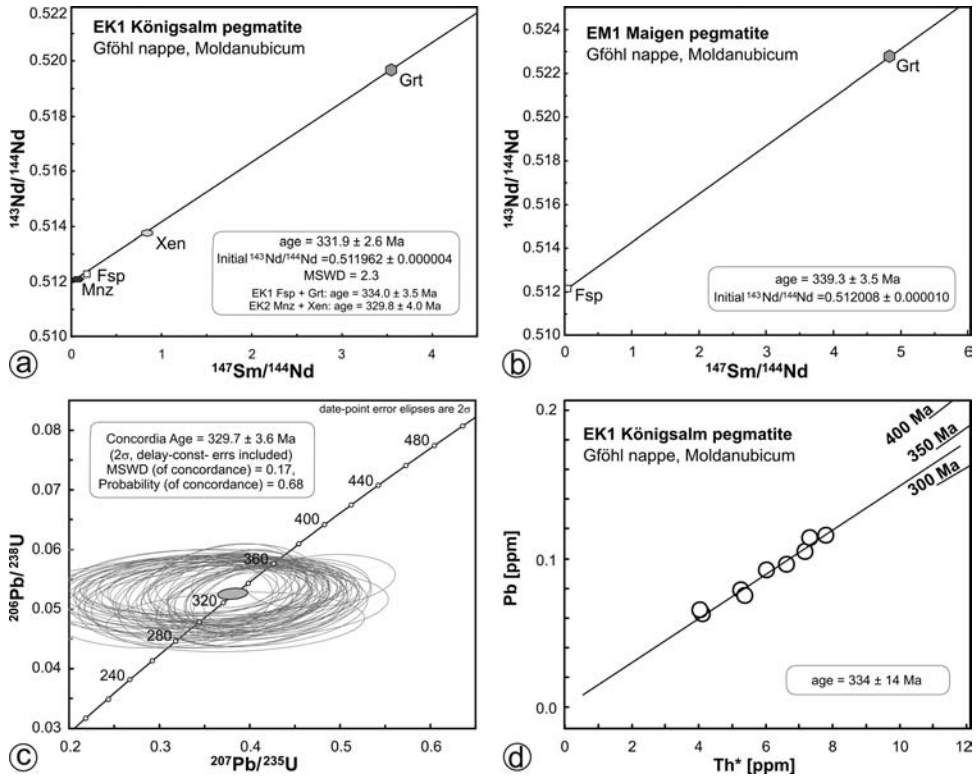

Fig. 7. Age diagrams for samples from the Königsalm (EK1, EK2) and Maigen (EM1) pegmatite (Moldanubic nappes in Lower Austria). (a) Sm-Nd isochron diagram including albite and garnet of sample ME1. Abbreviations: Grt – garnet, Fsp – feldspar, Mnz – monazite, Xen – xenotime. (c) Concordia diagram showing 62 *in-situ* laser ablation MC-ICP-MS U-Pb data points from 6 different monazite fragments from the Königsalm pegmatite (Moldanubian nappes, Lower Austria). The analyses define a concordia age of 330 ± 4 Ma. d) Th* versus Pb isochron diagram after Suzuki *et al.* (1991) showing data for monazite from the Königsalm pegmatite (Moldanubian nappes, Lower Austria). The analyses define a model isochron (forced through zero) with a weighted average age of 334 ± 14 Ma (95 % c.l.).

<*Z*-O> bond length. During the process of developing accurate formulae (using EMPA, SIMS and Mössbauer data) for tourmalines from the pegmatitic rocks described herein, we had similar difficulties. However, with Mg-rich tourmaline samples from the Rappold Complex of the Austroalpine nappes (Styria, Austria), Ertl *et al.* (2009) were very successful in developing accurate formulae. We attribute the difference to the varying *T*-site occupancy in the tourmalines from the Austroalpine nappes and the Moldanubicum, and suggest a relationship between *T*-site occupancy and the <*Z*-O> bond length. Whereas all tourmalines from the Austroalpine nappes show a <*T*-O> distance of 1.620 Å, the tourmalines from the Moldanubicum have varying <*T*-O> distances in the range 1.614–1.623 Å. This variation is a result of a mixed occupancy of Si, Al and B at the *T* site in tourmalines from the Moldanubicum, whereas in the samples from the Austroalpine nappes the *T* site is exclusively occupied by Si (Ertl *et al*., 2009).

Hence, we checked the possibility of an influence of the <*T*-O> bond length on the <*Z*-O> bond length. To ensure that the *Z* site is occupied by Al_6, only samples of the elbaite-olenite-rossmanite series were used (references see Fig. 8a). A positive correlation was observed between the <*T*-O> and <*Z*-O> bond lengths in tourmalines where the *Z* site is occupied by Al_6 without significant amounts of Fe, Mn, Mg and Ti at the *Z* site (58 samples, $R^2 = 0.617$; Fig. 8a). This is not unexpected, because the TO_4 tetrahedron is connected through two oxygens (O6 and O7) to the ZO_6 octahedron.

The influence of the <*T*-O> bond length on the <*Z*-O> distance (for a *Z* site that is only occupied by Al) can then be calculated as (1): $<Z\text{-O}>_{Al} = (<T\text{-O}>_{meas.} + 1.0439\ Å)/1.3961$ (Fig. 8a). Using this formula, the <*Z*-O> bond length for a *T* site only occupied with Si (corrected for the inductive effect of the varying <*T*-O> bond length) could be calculated for all tourmaline samples from the Moldanubicum using the formula (2): $<Z\text{-O}>_{calc.} = <Z\text{-O}>_{meas.} + 1.9078\ Å - <Z\text{-O}>_{Al}$. The value of 1.9078(6) Å was calculated for a <*Z*-O> distance for a Z site that is only occupied by Al and where the *T* site is only occupied by Si, as shown by using the average value of the <*T*-O> bond lengths of tourmalines characterised by Ertl *et al.* (2010a), because of the high-quality structure refinements reported therein ($R1$ = 0.013–0.015; standard deviations for <*T*-O> are ±0.0007–0.0008 Å). Finally, *Z*-site cations were assigned by optimising the relation between the <*Y*-O> bond length and the average ionic radius of the *Y*-site occupants (Fig. 8b) and also between $<Z\text{-O}>_{calc.}$ bond length and the average ionic radius of the *Z*-site occupants (Fig. 8c). The final assigned formulae for both relationships show excellent R^2 values of 0.994–0.998 (Fig. 8b) and 0.996 (Fig. 8c). Although we have only a limited number of samples, the correlation for *X*-site vacancy-rich tourmalines (≥0.4 vacancy per formula unit) shifts significantly towards a higher average ionic radius of the *Y*-site occupants. A possible explanation for this observation might be that the *Y* polyhedra share two oxygens (O2) with the *X* polyhedra (Table 3). Octahedrally coordinated vacancies were assigned to the *Y* site as it was proposed in the larger octahedron by Fortier & Donnay (1975), Foit & Rosenberg (1974) and proven by Ertl *et al.* (2006). The final simplified formulae of the tourmalines from the Moldanubian nappes are given in the section *Mineral compositions* and the detailed site occupations are given in Table 5.

To quantify Al-Mg disorder ($\delta_{Al\text{-}Mg}$) between the *Y* and the *Z* site, occupancies of these sites have to be known. A tourmaline with $^{Y}Mg_3$ and $^{Z}Al_6$ is perfectly ordered and hence $\delta_{Al\text{-}Mg} = 0$. A sample with $^{Y}(Al_2Mg)$ and $^{Z}(Al_4Mg_2)$ shows the strongest possible disorder ($\delta_{Al\text{-}Mg} = 1$). The Al-Mg disorder can be calculated as $\delta_{Al\text{-}Mg} = {}^{Z}Mg/(2\,{}^{Y}Mg)$. Late-stage crystallising Mg-bearing and *X*-site vacancy-rich tourmalines (foitite, magnesiofoitite; all samples from small miarolitic cavities) from the Königsalm pegmatite all have a relatively similar value of $\delta_{Al\text{-}Mg}$ (0.2). The average value of the ^{Y}Al-^{Z}Mg disorder of the Mg-rich tourmalines from the Austroalpine basement units (Rappold Complex), Styria, Austria, is significantly higher ($\delta_{Al\text{-}Mg} = 0.3$; Ertl *et al.*, 2010a). These authors assumed that these tourmalines may have formed at temperatures ≥550°C. Mg-rich tourmalines from the Drosendorf unit, Lower Austria, of the Moldanubian nappes show the highest ^{Y}Al-^{Z}Mg disorder ($\delta_{Al\text{-}Mg} = 0.5$; Ertl *et al*., 2008b). These authors assume that such a strong disorder derived from a relatively high temperature (~750°C) during crystallisation. All tourmaline samples which were used for the calculation of $\delta_{Al\text{-}Mg}$ are crystallised at low to medium pressure, the amount of Fe^{3+} at the *Z* site is ≤1 % of a fully occupied site (≤0.06 apfu), MgO ≥3.0 wt%, FeO + MnO ≤9.0 wt%. All these data would be consistent with the observation that the late-stage tourmalines from the Moldanubian nappes, Lower Austria, show significantly lower $\delta_{Al\text{-}Mg}$ values.

The reported value *U*eq for O1 for samples TK12, MAP12, BLG1 and BLP1 is significantly larger than the reported values for the other oxygen atoms (Table 2). Burns *et al.* (1994) observed the same feature in Mn-rich tourmalines and proposed that this could be related to positional disorder. A high negative correlation can be observed between the F content and the *X*-site vacancy in the tourmalines from the Moldanubicum ($R^2 = 0.930$; Fig. 8d). Similar correlations were described from Li-bearing tourmalines from Wolkenburg, Saxony, Germany, by Ertl *et al.* (2009) as well as from the Himalaya Mine, California, U.S.A., by Ertl *et al.* (2010c); Henry & Dutrow (2011) stated that petrologic factors superimpose the local environment on F concentrations. They also suggested that, within crystallographic constraints, local mineral assemblages and fractionating magmas/fluids control the amount of F that can be made available for incorporation in tourmaline. Ertl *et al.* (2010c) found an excellent negative correlation between the F content and the temperature conditions of ultra high pressure (UH*P*) tourmaline formation ($R^2 = 0.97$–1.00; chemical, structural data, respectively). We assume that temperature is also an important factor for the F incorporation in the tourmaline structure during crystallisation in low- to medium-pressure conditions. However, because of an increasing component of $^{[4]}Al$, related to an increasing formation temperature (Henry & Dutrow, 1996), such tourmalines might show a positive correlation between F content and the formation

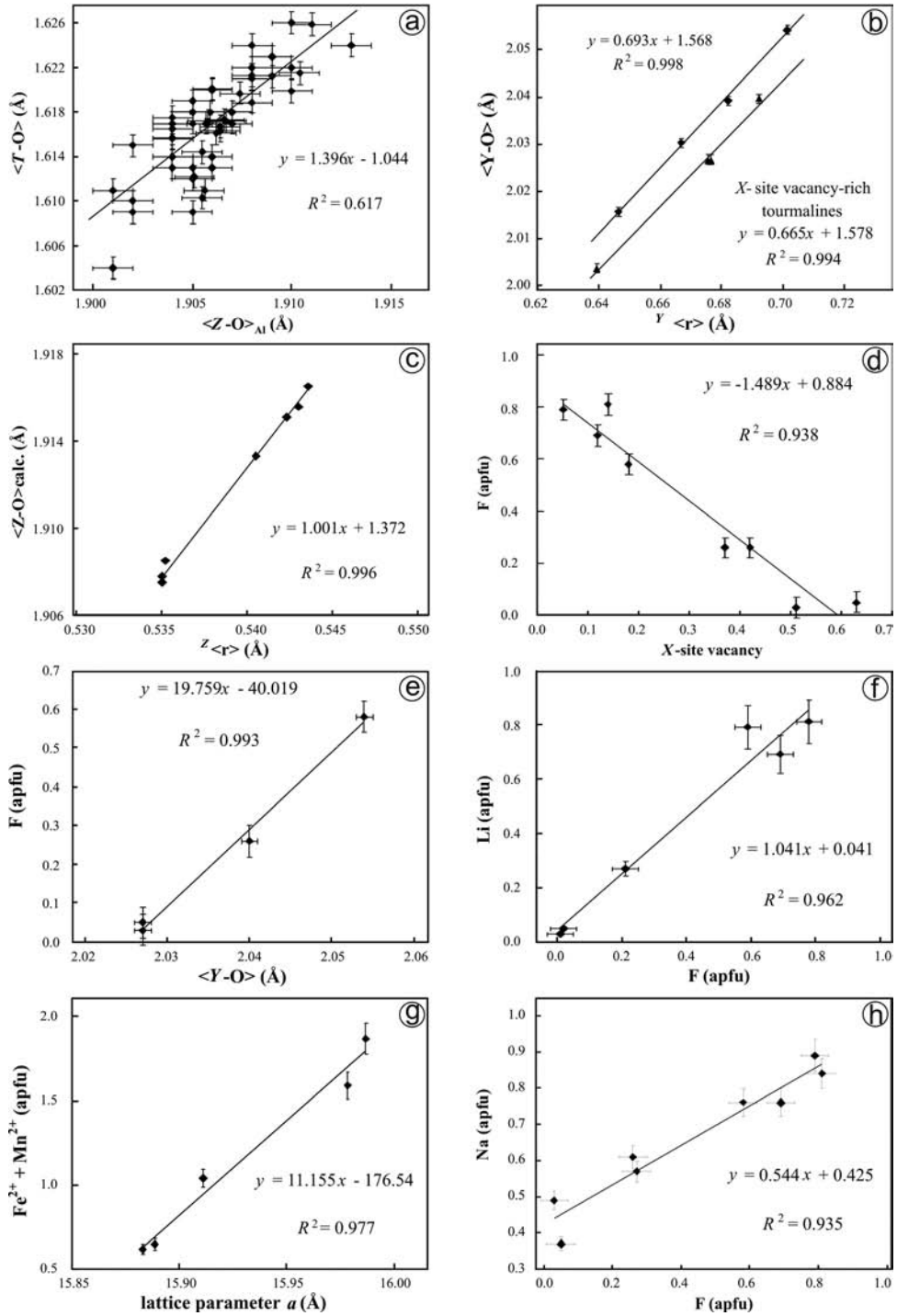

Fig. 8. Crystallographic and chemical relationships for tourmalines from different localities (Fig. 8a) and Moldanubian tourmalines from pegmatitic rocks of the Moldanubicum, Lower Austria (this study; Figs. 8b-8h; details see text). Bars = average standard deviation ($\pm 1\sigma$). (a) Influence of the average *T*-O bond length (Å) on the average *Z*-O bond length (Å), when the *Z* site is occupied by Al_6 (no Fe and Mn at the *Z* site) in (natural) tourmalines of the elbaite-olenite-rossmanite series. Plot of 58 samples with MgO $\leq$0.6 wt% and TiO_2 $\leq$0.3 wt% to exclude the possibility of significant amounts of Mg and Ti at the *Z* site (Burns *et al*., 1994; Selway *et al*., 1998; Hughes *et al*., 2000; Schreyer *et al*., 2002; Ertl *et al*., 2003a, 2004a and b, 2005, 2006, 2007, 2008a, 2009, 2010c; Prowatke *et al*., 2003; Bosi *et al*., 2005a and b; Cempírek *et al*., 2006; Lussier *et al*., 2008, 2011a and b). (b) Relationship between the average *Y*-O bond length (Å) and the average ionic radius of the *Y*-site occupants (Å). (c) Relationship between the calculated average *Z*-O bond length (Å) (see formula (2) under *Discussion*; corrected for the inductive effect of the varying <*T*-O> bond length; see Fig. 8a) and the average ionic radius of the *Z*-site occupants (Å). (d) Correlation between the F content and the *X*-site vacancy. (e) Fluorine (*apfu*) *vs*. <*Y*-O>; valid for all tourmalines from the Moldanubicum with Li_2O $\leq$0.1 wt%. (f) Lithium (*apfu*) *vs*. F (*apfu*); valid for all tourmalines from the Moldanubicum with FeO_{total} $\leq$9 wt%. (g) ($Fe^{2+} + Mn^{2+}$) *vs*. *a*; valid for all tourmalines from the Moldanubicum with $\leq$1.6 wt% MgO and <0.3 apfu $^{[4]}$B. (h) Relationship between Na and F content.

temperature when F is available for incorporation (Henry & Dutrow, 1996, 2011).

The three investigated tourmalines from the Königsalm pegmatite display a negative correlation between the *X*-site vacancies and the content of $^{[4]}$Al ($R^2 = 0.957$). Tourmalines with higher *X*-site vacancies (magnesiofoitite, foitite) have almost no Al at the *T* site (Table 4), which suggests formation temperatures <450 °C (Henry & Dutrow, 1996). This would be in agreement with a proposed late hydrothermal origin (200–300 °C) of magnesiofoitite and foitite (Hawthorne *et al*., 1999; Selway *et al*., 1999; Novák *et al*., 2004). A highly positive correlation between $^{[4]}$Al and ($Fe^{2+} + Mn^{2+}$) was found in tourmalines from the Himalaya Mine, California, U.S.A., by Ertl *et al.* (2010c). This relationship suggests that increasing formation temperatures exist for tourmalines with increasing ($Fe^{2+} + Mn^{2+}$) contents. This is supported by a positive correlation between ($Fe^{2+} + Mn^{2+}$) and Ti in the tourmalines ($R^2 = 0.717$) from the Moldanubian nappes. An increase in Ti as a function of increasing temperature (Thomson, 2006) is a trend observed in natural tourmaline. The UH*P* tourmalines described by Ertl *et al.* (2010b) display a strong positive correlation ($R^2 = 0.995$) between F content and <*Y*-O> distance. The tourmalines from the Moldanubicum, which are relatively low in Li ($Li_2O \leq 0.1$ wt%), also show a very high positive correlation ($R^2 = 0.993$; Fig. 8e). Samples with Li_2O contents in the range 0.3–1.2 wt% also show such a positive correlation ($R^2 = 0.789$). If F content is dependent on the temperature conditions of formation, this would have a direct influence to *Y*-site occupation, which is reflected by the the <*Y*-O> distance.

Another strong positive correlation in tourmalines (with $FeO_{total} \leq 9$ wt%) of the Moldanubian nappes was found between the Li and F content ($R^2 = 0.962$; Fig. 8f). Such a relationship is common, but is believed to be mainly dependent on petrologic factors (summarised by Ertl *et al*., 2010c). Also, simultaneous crystallisation of lepidolite can result in a decrease in F content as a consequence of a preferential partition into lepidolite relative to tourmaline (Ertl *et al*., 2010c).

A relation between the lattice parameter *a* and ($Fe^{2+} + Mn^{2+}$) content was noted by Ertl *et al.* (2010c) for samples from the schorl-elbaite solid solution from the Himalaya Mine, California. Another strong positive correlation, similar to that from the Himalaya Mine tourmalines, was found for all tourmalines from the Moldanubicum with ≤1.6 MgO and <0.3 apfu $^{[4]}$B ($R^2 = 0.977$; Fig. 8g). Hence, we believe that this correlation is of general usefulness for samples of the elbaite-schorl series with relatively low components of dravite, foitite and olenite, in which the olenite component is usually associated with the occurrence of $^{[4]}$B (*e.g*., Ertl *et al*., 2007, 2008a).

5.2. Chemical characteristics of Li-bearing tourmalines in different types of pegmatites

Selway *et al.* (1999) investigated Li-bearing tourmalines from the Czech Republic and from Red Cross Lake, Manitoba (Canada), and found several correlations between the chemical composition of the tourmalines and the type of the hosting pegmatite. Elbaite from lepidolite-subtype pegmatites is Ca and Mn-poor (<0.03 apfu Ca and <0.30 apfu Mn), whereas tourmaline from elbaite-subtype pegmatites is relatively Ca- and Mn-rich (<0.30 apfu Ca and <1.1 apfu Mn). Schorl in lepidolite-subtype pegmatites has extensive *X*-site vacancies, whereas schorl in elbaite-subtype pegmatites is Na-rich. There is a positive correlation between Na, Mn and F in tourmaline from lepidolite-subtype pegmatites.

Results from this study are in agreement with those from Selway *et al.* (1999) if the pegmatites are classified on the basis of the associated Li-minerals: tourmaline from the lepidolite-bearing pegmatite at Maigen is poor in Ca (0.01–0.02 apfu; Table 4) but can become relatively Mn-rich (up to 0.65 apfu Mn, elbaite MAP12; Table 4). Further, the schorl from the Maigen pegmatite is relatively rich in *X*-site vacancies (0.39 apfu, sample MASR; Table 4). In tourmalines from all investigated pegmatites of the Moldanubian nappes, a strong positive correlation ($R^2 = 0.935$) was found between Na and F (Fig. 8h). However, as already pointed out by Selway *et al.* (1999), this correlation is due to crystal-chemical constraints. Pronounced positive correlations were found between Mn^{2+} and Na ($R^2 = 0.639$) as well as between Mn^{2+} and F ($R^2 = 0.702$) only for the tourmalines from the lepidolite-bearing pegmatite at Maigen.

Selway *et al.* (1999) described late hydrothermal dark-violet foitite, with the formula $^{X}(\square_{0.61}Na_{0.39})$ $^{Y}(Fe^{2+}{}_{1.51}Al_{0.90}Li_{0.51}Mn^{2+}{}_{0.08})$ $^{Z}Al_6$ $(BO_3)_3$ $[Si_6O_{18}]$ $^{V}(OH)_3$ $^{W}(OH)$ (Li, B, H were calculated), which occurs as terminations on zoned tourmaline crystals in pockets of a lepidolite-subtype pegmatite at Dobrá Voda (Czech Republic part of the Moldanubicum). This composition is very similar, except for a significant Mg content, to our pink-to blue-coloured foitite (sample TK3; Tables 4 and 5), with the formula $^{X}(\square_{0.63}Na_{0.37})$ $^{Y}(Fe^{2+}{}_{1.12}Al_{1.09}Mg_{0.56}Mn^{2+}{}_{0.08}Fe^{3+}{}_{0.07}Li_{0.02}Ti^{4+}{}_{0.01}Zn_{0.01}\square_{0.04})$ $^{Z}(Al_{5.74}Mg_{0.26})$ $(BO_3)_3$ $[Si_{5.96}Al_{0.04}O_{18}]$ $^{V}(OH)_3$ $^{W}[(OH)_{0.95}F_{0.05}]$, from the Königsalm pegmatite. A similar Mg-bearing foitite (''oxy-foitite'' with ~0.27 apfu Mg) was described by Novák *et al.* (2004) from another lepidolite-subtype pegmatite (Bory pegmatite district, western Moravia, Czech Republic) of the Moldanubian nappes.

5.3. Genesis of the pegmatites in the regional framework

The pegmatites described in this paper crystallised in the Visean. An age of 339 ± 4 Ma has been determined for the Maigen sample, whereas the data set for the Königsalm pegmatite needs further examination. The latter pegmatite can be subdivided into different domains with individual mineral compositions and mineral chemistries that might have crystallised from melt fractions with differing isotopic signature or at different times. The isochrons of samples from two different domains (EK1 and EK2) yield somewhat different ages, but the ages, as well as the initial

$^{143}Nd/^{144}Nd$ ratios, are the same within the errors. Because of this result, it is likely that there was an isotopic equilibrium within the whole pegmatite and the pooled isochron age of 332 ± 3 Ma appears to be meaningful. In addition, the chemical Th-U-Pb ages as well as the concordia age of laser-ablation U-Pb ages for monazite of sample EK2 are in the same age range.

These ages determined for the pegmatites of Königsalm and Maigen are in good agreement with other published data for pegmatites of the Moldanubian nappes. A pegmatite from Eibenstein, which is situated in the Drosendorf unit intruded at 337 ± 5 Ma (Ertl *et al*., 2004b). For a potassic granulite, interpreted as a former pegmatitic dyke from the Moldanubian nappes (Gföhl nappe) at Plešovice (Czech Republic), an age of 337 ± 1 Ma was reported (Sláma *et al*., 2008) and for several other localities U-Pb ages on monazites of about 335 Ma were measured (Novák *et al*., 1998). On the basis of these data, pegmatite formation occurred in the Moldanubian nappes in the time span of 330–340 Ma.

The relationship between the genesis of the pegmatites and the South Bohemian Pluton is of interest. The intrusion sequence of the South Bohemian Pluton started with the coarse-grained peraluminous Rastenberg type durbachites (amphibole-biotite melasyenite to quartz melasyenite to melagranite with high K, Mg and Cr contents) at *ca*. 335 Ma, followed by Weinsberg type granites around 325 Ma (Klötzli *et al*., 1999). Both types of intrusions are characterised by initial ε_{Nd} and $^{87}Sr/^{86}Sr$ values in the range of –4.0 to –6.2 and 0.706–0.712, respectively. They are followed by the strongly peraluminous Eisgarn type granites (320–330 Ma, ε_{Nd} = –6.0 to –7.0; $^{87}Sr/^{86}Sr$ = 0.712 – 0.718), and a heterogeneous group represented by fine-grained, metaluminous or slightly peraluminous biotite-granites (type Mauthausen, Schrems, Altenberg, and Freistadt) (300–330 Ma; ε_{Nd} = –5.8 to –7.4; $^{87}Sr/^{86}Sr$ = 0.7053 – 0.7073) (Klötzli *et al*., 1999). As suggested by the ages, the pegmatites may have crystallised from differentiated melts of the Rastenberg type durbachites. According to Holub (1997) and Janoušek *et al.* (2003), the genesis of the latter is induced by processes in the mantle, including mantle delamination.

The initial ε_{Nd} values of the pegmatites from Königsalm (–4.9) and from Maigen (–3.8) are in agreement with this interpretation, whereas the initial ε_{Nd} value for the pegmatite of Eibenstein (–15.7; Ertl *et al*., 2004b; recalculated value) is significantly higher. Conversely, there are no spatial relationships between the outcrops of the Rastenberg type intrusions and the pegmatites. The area of the pegmatites investigated during this study is more than 10 km away from the intrusion of Rastenberg and there are no indications of an intrusive body in the subsurface of the investigated area (see also section in Fig. 1). Thus, it is not confirmed that the pegmatites crystallised from granitic-pegmatitic melts that evolved by fractionation from granitic parent melts, *e.g*. from the Rastenberg plutonic suite. Alternatively, they may represent relatively small volumes of decompression melts that did not move very far and that crystallised without passing through a stage of fractionation in a large granitic body. Such a pegmatite genesis was also proposed by Martin & De Vito (2005) and discussed by Simmons & Webber (2008). This speculation is supported by the occurrence of the pegmatites within partly migmatised gneisses of the Gföhl nappe and of the Drosendorf unit which experienced temperatures >700°C (Petrakakis, 1997).

The migmatisation is related to decompression of the upper amphibolite to granulite facies Moldanubian nappes during the exhumation after the metamorphic peak of the Variscan tectono-metamorphic event (Petrakakis *et al*., 1999). Abyssal pegmatites, which are related to anatectic processes, are common constituents of high-grade rocks in the Moldanubicum of the Bohemian Massif (Cempírek & Novák, 2007).

6. Conclusions

Coloured (brown, pink, green) tourmalines from three pegmatites from the Moldanubian nappes can be classified as fluor-schorl, schorl, foitite, magnesiofoitite, olenite and ''fluor-elbaite'' with varying Li (up to ~1.2 wt% Li_2O), F (up to ~1.6 wt%) and Mn contents (up to ~4.8 wt% MnO). These tourmalines are associated with quartz, plagioclase, microcline, garnet (spessartine-almandine), muscovite, biotite (annite), very rare lepidolite, apatite, monazite-(Ce), xenotime-(Y), allanite-(Ce) and zircon.

These tourmalines have <*T*-O> distances varying from 1.614 to 1.623 Å. There is a positive correlation between the <*T*-O> and <*Z*-O> bond lengths in tourmalines in which the *Z* site is only occupied by Al (R^2 = 0.617). By using the relation [$<Z\text{-O}>_{calc.} = <Z\text{-O}>_{meas.} + 1.9078$ Å – ($<T\text{-O}>_{meas.} + 1.0439$ Å)/1.3961], the <*Z*-O> bond length can be corrected for the inductive effect of the varying <*T*-O> bond length. This is important to produce accurate site assignments of the crystal chemical tourmaline formula, particularly for samples with Al-Mg disorder between the *Y* and the *Z* site. Such disorder is believed to be essentially dependent on the availability of Mg, on the temperature during tourmaline crystallisation (Ertl *et al*., 2008b), as well as on stereochemical constraints (Bosi, 2011).

Tourmaline is a common phase in the investigated pegmatites. It is likely that the crystallisation of tourmaline phases depleted the melt in boron and hence removed a fluxing component. Such a chemical quenching could initiate a rapid crystallisation of the pegmatitic components because the melt is no longer fluxed by that component (Simmons & Webber, 2008). This would be in agreement with the observation of tapered tourmaline crystals in the Königsalm and Maigen pegmatites.

The crystallisation age of the Maigen pegmatite is 339 ± 4 Ma, whereas that of the Königsalm pegmatite is 332 ± 3 Ma. These ages are in agreement with those from other pegmatites in the Moldanubian nappes, which are in the range of 330–340 Ma.

The time interval between 330 and 340 Ma covers only the earliest intrusions of the South Bohemian pluton, which are represented by the Rastenberg type durbachites. Melt generation of these intrusions is related to processes in the

mantle, and they crystallised at about 335 Ma (Holub, 1997; Klötzli *et al*., 1999; Janoušek *et al*., 2003). Even if the ε_{Nd} values of the pegmatites from Maigen and Königsalm are in accord with those of the Rastenberg type durbachites, those of other pegmatites are not, and there are no spatial relationships of the durbachites and the pegmatites. Therefore it is doubtful that the pegmatites evolved as differentiated melts from the Rastenberg type durbachites.

Alternatively, and in our opinion more likely, the pegmatitic melts may have formed by decompression melting of the hosting country rocks that are represented by the partly migmatised gneisses of the Gföhl nappe and the Drosendorf unit. In this case, the formation of the pegmatites would be related to the exhumation of the Moldanubian nappes after the peak of the Variscan metamorphic cycle at about 340 Ma.

Acknowledgements: Special thanks to Erwin Löffler for the tourmaline samples from Maigen, to Gerald Knobloch for the tourmaline samples from Blocherleitengraben and for detailed information about the localities, and to Gottfried Domanig for samples from Königsalm (tourmalines TK3, TK42, allanite). We are grateful to Andreas Wagner, Vienna, Austria, for sample preparation. We thank Monika Horschinegg, Department of Lithospheric Research, Vienna, Austria, for her help with the isotopic analyses and Richard Göd for references of the pegmatite classification. We sincerely thank Milan Novák and Ferdinando Bosi for their constructive reviews. This work was supported in part by Austrian Science Fund (FWF) project no. P23012-N19 (to AE) and the White Rose Foundation (to GRR); JMH gratefully acknowledges support from US NSF grant EAR-0003201.

References

Bloodaxe, E.S., Hughes, J.M., Dyar, M.D., Grew, E.S., Guidotti, C.V. (1999): Linking structure and chemistry in the Schorl-Dravite series. *Am. Mineral.*, **84**, 922–928.

Bosi, F. (2011): Stereochemical constraints in tourmaline: from a short-range to a long-range structure. *Can. Mineral.*, **49**, 17–27.

Bosi, F. & Lucchesi, S. (2004): Crystal chemistry of the schorl-dravite series. *Eur. J. Mineral.*, **16**, 335–344.

—,— (2007): Crystal chemical relationships in the tourmaline group: structural constraints on chemical variability. *Am. Mineral.*, **92**, 1054–1063.

Bosi, F., Agrosì, G., Lucchesi, S., Melchiorre, G., Scandale, E. (2005a): Mn-tourmaline from island of Elba (Italy): crystal chemistry. *Am. Mineral.*, **90**, 1661–1668.

Bosi, F., Andreozzi, G.B., Federico, M., Graziani, G., Lucchesi, S. (2005b): Crystal chemistry of the elbaite-schorl series. *Am. Mineral.*, **90**, 1784–1792.

Burns, P.C., MacDonald, D.J., Hawthorne, F.C. (1994): The crystal chemistry of manganese-bearing elbaite. *Can. Mineral.*, **32**, 31–41.

Carswell, D.A. (1991): Variscan high P-T metamorphism and uplift history in the Moldanubian Zone of the Bohemian Massif in Lower Austria. *Eur. J. Mineral.*, **3**, 323–342.

Carswell, D.A. & O'Brien, P.J. (1991): High pressure granulites in the Moldanubian Zone, Lower Austria. *Terra Abstr.*, **3**, 93.

—,— (1993): Thermobarometry and Geotectonic significance of High-Pressure Granulite examples from the Moldanubian Zone of the Bohemian Massif in Lower Austria. *J. Petrol.*, **34**, 427–459.

Cempírek, J. & Novák, M. (2007): Abyssal pegmatites in Moldanubicum of the Bohemian Massif. Granitic Pegmatites: The State of the Art – International Symposium, 6th–12th May 2007, Porto, Universidade do Porto, Faculdade de Ciencias, Portugal. Memórias, **8**, 34–35.

Cempírek, J., Novák, M., Ertl, A., Hughes, J.M., Rossman, G.R., Dyar, M.D. (2006): Fe-bearing olenite with tetrahedrally coordinated Al from an abyssal pegmatite of the Bohemian massif at Kutná Hora: structure, crystal chemistry, and optical spectra. *Can. Mineral.*, **44**, 23–30.

Dallmeyer, R.D., Neubauer, F., Höck, V. (1992): Chronology of late Paleozoic tectonothermal activity in the southeastern Bohemian Massif, Austria (Moldanubian and Moravo-Silesian zones): $^{40}Ar/^{39}Ar$ mineral age controls. *Tectonophysics*, **210**, 135–153.

Dyar, M.D., Taylor, M.E., Lutz, T.M., Francis, C.A., Robertson, J.D., Cross, L.M., Guidotti, C.V., Wise, M. (1998): Inclusive chemical characterization of tourmaline: Mössbauer study of Fe valence and site occupancy. *Am. Mineral.*, **83**, 848–864.

Ertl, A. (1995): Elbait, Olenit, Dravit-Buergerit-Mischkristalle, Dravit, Uvit und ein neuer Al-Turmalin (?) von österreichischen Fundstellen. *Mitt. Österr. Miner. Ges.*, **140**, 55–72.

Ertl, A., Hughes, J.M., Prowatke, S., Rossman, G.R., London, D., Fritz, E.A. (2003a): Mn-rich tourmaline from Austria: structure, chemistry, optical spectra, and relations to synthetic solid solutions. *Am. Mineral.*, **88**, 1369–1376.

Ertl, A., Hughes, J.M., Brandstätter, F., Dyar, M.D., Prasad, P.S.R. (2003b): Disordered Mg-bearing olenite from a granitic pegmatite from Goslarn, Austria: a chemical, structural, and infrared spectroscopic study. *Can. Mineral.*, **41**, 1363–1370.

Ertl, A., Pertlik, F., Dyar, M.D., Prowatke, S., Hughes, J.M., Ludwig, T., Bernhardt, H.-J. (2004a): Fe-rich olenite with tetrahedrally coordinated Fe^{3+} from Eibenstein, Austria: structural, chemical, and Mössbauer data. *Can. Mineral.*, **42**, 1057–1063.

Ertl, A., Schuster, R., Prowatke, S., Brandstätter, F., Ludwig, T., Bernhardt, H.-J., Koller, F., Hughes, J.M. (2004b): Mn-rich tourmaline and fluorapatite in a Variscan pegmatite from Eibenstein an der Thaya, Bohemian massif, Lower Austria. *Eur. J. Mineral.*, **16**, 551–560.

Ertl, A., Rossman, G.R., Hughes, J.M., Prowatke, S., Ludwig, T. (2005): Mn-bearing ''oxy-rossmanite'' with tetrahedrally-coordinated Al and B from Austria: structure, chemistry, and infrared and optical spectroscopic study. *Am. Mineral.*, **90**, 481–487.

Ertl, A., Hughes, J.M., Prowatke, S., Ludwig, T., Prasad, P.S.R., Brandstätter, F., Körner, W., Schuster, R., Pertlik, F., Marschall, H. (2006): Tetrahedrally-coordinated boron in tourmalines from the liddicoatite-elbaite series from Madagascar: structure, chemistry, and infrared spectroscopic studies. *Am. Mineral.*, **91**, 1847–1856.

Ertl, A., Hughes, J.M., Prowatke, S., Ludwig, T., Brandstätter, F., Körner, W., Dyar, M.D. (2007): Tetrahedrally-coordinated boron in Li-bearing olenite from ''mushroom'' tourmaline from Momeik, Myanmar. *Can. Mineral.*, **45**, 891–899.

Ertl, A., Tillmanns, E., Ntaflos, T., Francis, C., Giester, G., Körner, W., Hughes, J.M., Lengauer, C., Prem, M. (2008a): Tetrahedrally coordinated boron in Al-rich tourmaline and its relationship to the pressure–temperature conditions of formation. *Eur. J. Mineral.*, **20**, 881–888.

Ertl, A., Rossman, G.R., Hughes, J.M., Ma, C., Brandstätter, F. (2008b): V^{3+}-bearing, Mg-rich, strongly disordered olenite from a graphite deposit near Amstall, Lower Austria: A structural, chemical and spectroscopic investigation. *N. Jb. Mineral. Abh.*, **184**, 243–253.

Ertl, A., Kolitsch, U., Meyer, H.-P., Ludwig, T., Lengauer, C.L., Nasdala, L., Tillmanns, E. (2009): Substitution mechanism in tourmalines of the ''fluor-elbaite''-rossmanite series from Wolkenburg, Saxony, Germany. *N. Jb. Mineral. Abh.*, **186**, 51–61.

Ertl, A., Mali, H., Schuster, R., Körner, W., Hughes, J.M., Brandstätter, F., Tillmanns, E. (2010a): Li-bearing, disordered Mg-rich tourmalines from the pegmatite-marble contact from the Austroalpine basement units (Styria, Austria). *Mineral. Petrol.*, **99**, 89–104.

Ertl, A., Marschall, H.R., Giester, G., Henry, D.J., Schertl, H.-P., Ntaflos, T., Luvizotto, G.L., Nasdala, L., Tillmanns, E. (2010b): Metamorphic ultra high-pressure tourmalines: structure, chemistry, and correlations to PT conditions. *Am. Mineral.*, **95**, 1–10.

Ertl, A., Rossman, G.R., Hughes, J.M., London, D., Wang, Y., O'Leary, J.A., Dyar, M.D., Prowatke, S., Ludwig, T., Tillmanns, E. (2010c): Tourmaline of the elbaite-schorl series from the Himalaya Mine, Mesa Grande, California, U.S.A.: a detailed investigation. *Am. Mineral.*, **95**, 24–40.

Finger, F., Gerdes, A., Janoušek, V., René, M., Riegler, G. (2007): Resolving the Variscan evolution of the Moldanubian sector of the Bohemian Massif: the significance of the Bavarian and the Moravo-Moldanubian tectonometamorphic phases. *J. Geosci.*, **52**, 9–28.

Fischer, R.X. & Tillmanns, E. (1988): The equivalent isotropic displacement factor. *Acta Cryst. C*, **44**, 775–776.

Foit, Jr., F.F. & Rosenberg, P.E. (1974): Coupled substitutions in the tourmaline group. *Contrib. Mineral. Petrol.*, **62**, 109–127.

Fortier, S. & Donnay, G. (1975): Schorl refinement showing composition dependence of the tourmaline structure. *Can. Mineral.*, **13**, 173–177.

Frank, W., Hammer, St., Popp, F., Scharbert, S., Thöni, M. (1990): Isotopengeologische Neuergebnisse zur Entwicklungsgeschichte der Böhmischen Masse: Proterozoische Gesteinsserien und Variszische Hauptorogenese. *Österr. Beitr. Met. Geoph.*, **3**, 185–228.

Frank, W. & Scharbert, S. (1993): K/Ar und $^{40}Ar/^{39}Ar$-Daten von Glimmern der Böhmischen Masse, Projekt S4702. *Mitt. Österr. Miner. Ges.*, **138**, 119–122.

Friedl, G., von Quadt, A., Ochsner, A., Finger, F. (1993): Timing of the Variscan orogeny in the Southern Bohemian Massif (NE Austria) deduce from new U-Pb monazite and zircon dating. *Terra Abs.*, **1**, 235.

Fuchs, G. & Matura, A. (1976): Zur Geologie des Kristallins der Böhmischen Masse. *Jb. Geol. B.-A.*, **119**, 1–43.

Grice, J.D. & Ercit, T.S. (1993): Ordering of Fe and Mg in the tourmaline crystal structure: the correct formula. *N. Jb. Mineral. Abh.*, **165**, 245–266.

Hawthorne, F.C., MacDonald, D.J., Burns, P.C. (1993): Reassignment of cation site-occupancies in tourmaline: Al-Mg disorder in the crystal structure of dravite. *Am. Mineral.*, **78**, 265–270.

Hawthorne, F.C., Selway, J.B., Kato, A., Matsubara, S., Shimizu, M., Grice, J.D., Vajdak, J. (1999): Magnesiofoitite, □ (Mg_2Al) Al_6 (Si_6O_{18}) $(BO_3)_3$ $(OH)_4$, a new alkali-deficient tourmaline. *Can. Mineral.*, **37**, 1439–1443.

Hehenberger, R. (1996): Vergleichende mineralogische Untersuchungen an granatführenden Pegmatiten (Almandin-Spessartin-Mischkristalle) im südl. Moldanubikum, NÖ. Master thesis, Univ. Wien, 207 p.

Henry, D.J. & Dutrow, B.L. (1996): Metamorphic tourmaline and its petrologic applications. in ''Boron: Mineralogy, Petrology, and Geochemistry'', E.S. Grew & L.M. Anovitz, eds., *Rev. Mineral. Geochem.*, **33**, Mineralogical Society of America, Chantilly, VA, 503–557.

—,— (2011): The incorporation of fluorine in tourmaline: internal crystallographic controls or external environmental influences? *Can. Mineral.*, **49**, 41–56.

Henry, D.J., Novák, M., Hawthorne, F.C., Ertl, A., Dutrow, B.L., Uher, P., Pezzotta, F. (2011): Nomenclature of the tourmaline-supergroup minerals. *Am. Mineral.*, **96**, 895–913.

Himmelbauer, A. (1929): Vorlage neuer Mineralvorkommen aus Niederösterreich und dem Burgenland. *Mitt. Wiener Min. Ges.*, **92**, 5–7. In: *Tscherm. Min. Petr. Mitt.*, N. F. 19.

Holub, F.V. (1997): Ultrapotassic plutonic rocks of the Durbachite Series in the Bohemian Massif; petrology, geochemistry and petrogenetic interpretation. *Sbor. Geol. Věd, Ložisk. Geol. Mineral.*, **31**, 5–26.

Huber, P. & Huber, S. (1977): Mineralfundstellen in Oberösterreich, Niederösterreich und Burgenland. Christian Weise Verlag, München, 270 p.

Hughes, J.M., Ertl, A., Dyar, M.D., Grew, E.S., Shearer, C.K., Yates, M.G., Guidotti, C.V. (2000): Tetrahedrally coordinated boron in a tourmaline: boron-rich olenite from Stoffhütte, Koralpe, Austria. *Can. Mineral.*, **38**, 861–868.

Janoušek, V., Holub, F.V., Gerdes, A. (2003): K-rich magmatism in the Moldanubian Unit, Bohemian Massif – a complex story featuring variably enriched lithospheric mantle melts and their interaction with the crust. *Geolines*, **16**, 48–49.

Kappelmüller, H. (1994): Mineralfundstellen in Niederösterreich. Bode Verlag, Haltern, 72 p.

Klötzli, U., Frank, W., Scharbert, S., Thöni, M. (1999): Evolution of the SE Bohemian Massif based on geochronological data – a review. *Jb. Geol. B.-A.*, **141**, 377–394.

Klötzli, U., Klötzli, E., Günes, Z., Košler, J. (2009): External accuracy of laser ablation U-Pb zircon dating: results from a test using five different reference zircons. *Geostand. Geoanal. Res.*, **33**, 1, 5–15.

Knobloch, G. (1982): Roter Turmalin aus dem Waldviertel. *Lapis*, **7**, 12, 34.

Kontrus, K. & Niedermayr, G. (1969): Neue Mineralfunde aus Österreich, 1962–1968. *Tscherm. Min. Petr. Mitt.*, 3. Folge, **13**, 355–359.

Koller, F. (1974): Einige neue Mineralfunde im Waldviertel. *Mitt. Österr. Min. Ges.*, **124**, 14–16.

Krenn, E., Ustaszewski, K., Finger, F. (2008): Detrital and newly formed metamorphic monazite in amphibolite-facies metapelites from the Motajica Massif, Bosnia. *Chem. Geol.*, **254**, 164–174.

Kroner, U., Mansky, J.-L., Mazur, S., Aleksandrowski, P., Hann, H.P., Huckride, H., Lacquement, F., Lamarche, J., Ledru, P., Pharaoh, T.C., Zedler, H., Zeh, A., Zulauf, G. (2008): Variscan tectonics. *in* ''The Geology of Central Europe. Volume 1: Precambrian and Palaeozoic'', T. McCann, ed., Geological Society, London, 599–664.

Linner, M. (2007): Das Bavarikum - eine tektonische Einheit im südwestlichen Moldanubikum (Böhmische Masse). *Arbeitstagung Geol. B.-A.*, **2007**, 173–176.

Long, G.J., Cranshaw, T.E., Longworth, G. (1983): The ideal Mössbauer effect absorber thickness. *Mössbauer Effect Ref. Data J.*, **6**, 42–49.

Ludwig, K.R. (2003): Isoplot/Ex Version 3.0. A Geochronological Toolkit for Microsoft Excel. Berkeley Geochronological Centre Special Publication, Berkeley, 70 p.

Lussier, A.J., Aguiar, P.M., Michaelis, V.K., Kroeker, S., Herwig, S., Abdu, Y., Hawthorne, F.C. (2008): Mushroom elbaite from the Kat Chay mine, Momeik, near Mogok, Myanmar: I. Crystal chemistry by SREF, EMPA, MAS NMR and Mössbauer spectroscopy. *Mineral. Mag.*, **72**, 747–761.

Lussier, A.J., Abdu, Y., Hawthorne, F.C., Michaelis, V.K., Aguiar, P.M., Kroeker, S. (2011a): Oscillatory zoned liddicoatite from Anjanabonoina, central Madagascar. I. Crystal chemistry and structure by SREF and ^{11}B and ^{27}Al MAS NMR spectroscopy. *Can. Mineral.*, **49**, 63–88.

Lussier, A.J., Hawthorne, F.C., Abdu, Y., Herwig, S., Michaelis, V.K., Aguiar, P.M., Kroeker, S. (2011b): The crystal chemistry of 'wheatsheaf' tourmaline from Mogok, Myanmar. *Mineral. Mag.*, **75**, 65–86.

Martin, R.F. & De Vito, C. (2005): The patterns of enrichment in felsic pegmatites ultimately depend on tectonic setting. *Can. Mineral.*, **43**, 2027–2048.

Mattson, S.M. & Rossman, G.R. (1987): Fe^{2+}-Fe^{3+} interactions in tourmaline. *Phys. Chem. Minerals*, **14**, 163–171.

—,— (1988): Fe^{2+}-Ti^{4+} charge transfer absorption in stoichiometric Fe,Ti minerals. *Phys. Chem. Minerals*, **16**, 78–82.

Matura, A. (2003): Zur tektonischen Gliederung der variszischen Metamorphite im Waldviertel Niederösterreichs. *Jb. Geol. B.-A.*, **143**, 221–225.

Medaris, L.G., Wang, H.F., Mísar, Z., Jelínek, E. (1990): Thermobarometry, diffusion modeling and cooling rates of crustal garnet peridotites: two examples from the Moldanubian zone of the Bohemian Massif. *Lithos*, **25**, 189–202.

Meixner, H. (1965): Xenotim-Kristalle von Königsalm a.d. Krems bei Senftenberg, NÖ. *Carinthia II*, **155**, 75, 75–77.

Meixner, H. (1981): Fast farbloser bis bläulicher Turmalinasbest von der Königsalm/NÖ. *Carinthia II*, 171/91. 51.

Montel, J.M., Foret, S., Veschambre, M., Nicollet, C., Provost, A. (1996): Electron microprobe dating of monazite. *Chem. Geol.*, **131**, 37–53.

Niedermayr, G. (1969): Der Pegmatit der Königsalm, Niederösterreich. *Ann. Naturhist. Mus. Wien*, **73**, 49–54.

Neubauer, F. & Handler, R. (2000): Varican orogeny in the Eastern Alps and Bohemian Massif: how do these units correlate. *Mitt. Österr. Geol. Ges.*, **92**, 35–59.

Novák, M. & Povondra, P. (1995): Elbaite pegmatites in the Moldanubicum: a new subtype of the rare-element class. *Mineral. Petrol.*, **55**, 159–176.

Novák, M., Černý, P., Kimbrough, D.L., Taylor, M.C., Ercit, T.S. (1998): U-Pb Ages of monazite from granitic pegmatits in the Moldanubian Zone and their geological implications. *Acta Univ. Carol.*, Vol. conf. POCEEL Praha, **42**, 309–310.

Novák, M., Selway, J.B., Černý, P., Hawthorne, F.C., Ottolini, L. (1999): Tourmaline of the elbaite-dravite series from an elbaite-subtype pegmatite at Bližná, southern Bohemia, Czech Republic. *Eur. J. Mineral.*, **11**, 557–568.

Novák, M., Povondra, P., Selway, J. (2004): Schorl-*oxy-schorl* to dravite-*oxy-dravite* tourmaline from granitic pegmatites; examples from the Moldanubicum, Czech Republic. *Eur. J. Mineral.*, **16**, 323–333.

Petrakakis, K. (1997): Evolution of Moldanubian rocks in Austria. *J. Metamorphic. Geol.*, **15**, 203–223.

Petrakakis, K., Klötzli, U., Richter, W. (1999): Excursion to the Austrian part of Moldanubia. *Beih. z. Eur. J. Mineral.*, **11**, 61–90.

Prince, C., Košler, J., Vance, D., Günther, D. (2000): Comparison of laser ablation ICP-MS and isotope dilution REE analyses – implications for Sm-Nd garnet geochronology. *Chem. Geol.*, **168**, 255–274.

Prowatke, S., Ertl, A., Hughes, J.M. (2003): Tetrahedrally-coordinated Al in Mn-rich, Li- and Fe-bearing olenite from Eibenstein an der Thaya, Lower Austria: a chemical and structural investigation. *N. Jb. Mineral. Mh.*, **2003**, 385–395.

Reinitz, I.M. & Rossman, G.R. (1988): The role of natural radiation in tourmaline coloration. *Am. Mineral.*, **73**, 822–825.

Schreyer, W., Hughes, J.M., Bernhardt, H.-J., Kalt, A., Prowatke, S., Ertl, A. (2002): Reexamination of olenite from the type locality: detection of boron in tetrahedral coordination. *Eur. J. Mineral.*, **14**, 935–942.

Selway, J.B., Hawthorne, F.C., Černý, P., Ottolini, L., Novák, M., Kyser, T.K. (1998): Rossmanite, $\square(LiAl_2)Al_6(Si_6O_{18})(BO_3)_3(OH)_4$, a new alkali-deficient tourmaline: description and crystal structure. *Am. Mineral.*, **83**, 896–900.

Selway, J.B., Novák, M., Černý, P., Hawthorne, F.C. (1999): Compositional evolution of tourmaline in lepidolite-subtype pegmatites. *Eur. J. Mineral.*, **11**, 569–584.

Sigmund, A. (1937): Die Minerale Niederösterreichs. 2nd ed., F. Deuticke, Wien und Leipzig, 247 p.

Simmons, W.B. & Webber, K.L. (2008): Pegmatite genesis: state of the art. *Eur. J. Mineral.*, **20**, 421–438.

Sláma, J., Košler, J., Condon, D.J., Crowley, J.L., Gerdes, A., Hanchar, J.M., Horstwood, M.S.A., Morris, G.A., Nasdala, L., Norberg, N., Schaltegger, U., Schoene, B., Tubrett, M.N., Whitehouse, M.J. (2008): Plešovice zircon – A new natural reference material for U–Pb and Hf isotopic microanalysis. *Chem. Geol.*, **249**, 1–35.

Smith, G. (1977): Low-temperature optical studies of metal-metal charge-transfer transitions in various minerals. *Can. Mineral.*, **15**, 500–507.

Sölva, H., Grasemann, B., Thöni, H., Thiede, R., Habler, G. (2005): The Schneeberg Normal Fault Zone : Normal faulting associated with Cretaceous SE-directed extrusion in the Eastern alps (Italy/Austria). *Technophysics*, **401**, 143–166.

Suzuki, K., Adachi, M., Tanaka, T. (1991): Middle Precambrian provenance of Jurassic sandstone in the Mino Terrane, central Japan: Th-U-total Pb evidence from an electron microprobe monazite study. *Sediment. Geol.*, **75**, 141–147.

Svojtka, M., Košler, J., Venera, Z. (2002): Dating granulite-facies structures and the exhumation of lower crust in the Moldanubian Zone of the Bohemian Massif. *Int. J. Earth Sci. (Geol. Rundsch.)*, **91**, 373–385.

Thomson, J.A. (2006): A rare garnet-tourmaline-sillimanite-biotite-ilmenite-quartz assemblage from the granulite facies of south-central Massachusetts. *Am. Mineral.*, **91**, 1730–1738.

Tropper, P., Deibl, I., Finger, F., Kaindl, R. (2006): P–T–t evolution of spinel-cordierite-garnet gneisses from the Sauwald Zone (Southern Bohemian Massif, Upper Austria): is there evidence for two independent late-Variscan low-P/high-T events in the Moldanubian Unit? *Int. J. Earth Sci.*, **95**, 1019–1037.

Wivel, C. & Mørup, S. (1981): Improved computational procedure for evaluation of overlapping hyperfine parameter distributions in Mössbauer spectra. *J. Phys. E: Sci. Instr.*, **14**, 605–610.

Received 4 May 2011
Modified version received 27 October 2011
Accepted 13 February 2012